JAMES | Journal of Advances in Modeling Earth Systems®

RESEARCH ARTICLE
10.1029/2022MS003385

Linking Biogeochemical and Hydrodynamic Processes to Model Methane Fluxes in Shallow, Tropical Floodplain Lakes

Mingyang Guo[1], John M. Melack[2,3], Wencai Zhou[2], Pedro M. Barbosa[2,4], Joao H. F. Amaral[2,5], and Qianlai Zhuang[1]

[1]Department of Earth, Atmospheric and Planetary Sciences, Purdue University, West Lafayette, IN, USA, [2]Earth Research Institute, University of California, Santa Barbara, CA, USA, [3]Bren School of Environmental Science and Management, University of California, Santa Barbara, CA, USA, [4]Département des Sciences Biologiques, Groupe de Recherche Interuniversitaire en Limnologie, Université du Québec à Montréal, Montreal, QC, Canada, [5]Faculty of Natural Sciences, Earth System Science Program, Universidad del Rosario, Bogota, Colombia

Key Points:

- Methane fluxes from Amazon floodplains lakes simulated with biogeochemical model combined with hydrodynamic model
- Seasonal patterns and magnitudes of simulated and measured fluxes are generally in good agreement
- Methane concentrations and diffusive emissions are sensitive to carbon mineralization and methane production and oxidation

Supporting Information:

Supporting Information may be found in the online version of this article.

Correspondence to:

J. M. Melack,
john.melack@lifesci.ucsb.edu

Citation:

Guo, M., Melack, J. M., Zhou, W., Barbosa, P. M., Amaral, J. H. F., & Zhuang, Q. (2023). Linking biogeochemical and hydrodynamic processes to model methane fluxes in shallow, tropical floodplain lakes. *Journal of Advances in Modeling Earth Systems*, *15*, e2022MS003385. https://doi.org/10.1029/2022MS003385

Received 4 SEP 2022
Accepted 14 NOV 2023

Author Contributions:

Conceptualization: John M. Melack, Qianlai Zhuang
Data curation: John M. Melack, Wencai Zhou
Formal analysis: Mingyang Guo, Wencai Zhou
Funding acquisition: John M. Melack, Qianlai Zhuang

Abstract

Floodplains lakes are abundant in the Amazon basin and are important methane sources to the atmosphere. Existing biogeochemical models require modifications and inclusion of hydrodynamic processes operative in shallow, warm waters to be applied to these aquatic ecosystems. We modified a 1-dimensional process-based, lake biogeochemical model and combined a 3-dimensional hydrodynamic model to suit Amazon floodplains. We evaluated the combined model's performance simulating methane concentrations and fluxes and several related processes in the open lake and an embayment of a well-studied Amazon lake. Parameters for calibration were selected through sensitivity tests using a machine learning-based algorithm, classification, and regression trees. Comparison between simulated and measured fluxes indicate generally good agreement in seasonal patterns and magnitudes. Comparisons of near-surface concentrations varied with no clear patterns. Simulations of methane concentrations at near-surface and near-bottom, and diffusive emissions are most sensitive to carbon mineralization rate, Q_{10} factors for methanogenesis and oxidation, and methane oxidation potential. Modeled rates of planktonic photosynthesis were generally lower than measurements, though simulated planktonic respiration was often similar to measurements. Simulated rates of methane oxidation were considerably lower, with a few exceptions, than measurements of methane oxidation in oxic water of the lake. Improvements of results of the linked hydrodynamic-biogeochemical model will result from inclusion of advective transport, use of parameter values appropriate for tropical waters, especially for methane oxidation and photosynthesis, and addition of changes in hydrostatic pressure to model of ebullition.

Plain Language Summary

Methane emissions from lakes are large, highly variable and without adequate measurements, especially in tropical regions. The combination of mechanistic models with results from intensive field data provides one way to improve understanding of the processes and sources of variability. Riverine floodplain lakes, as occur in the Amazon basin, constitute extensive aquatic ecosystems and are important methane sources to the atmosphere. Though tropical lakes typically experience muted seasonal variations in climate, strong diel changes occur, and floodplain lakes have additional biogeochemical and ecological variability caused by changes in water level, connectivity to rivers and optical properties. We modified a one-dimensional process-based, lake biogeochemical model and combined a 3-dimensional hydrodynamic model to be applicable to Amazon floodplains and similar shallow, warm waters. The combined model simulated well methane processes and fluxes based on evaluation using observations in a representative central Amazon floodplain lake with measurements of meteorological variables, water temperatures and ecological conditions, and methane emissions over the seasonal hydrological phases with large differences in water levels.

1. Introduction

Estimates of methane emissions from lakes are large with high temporal and spatial variability (Rosentreter et al., 2021). The considerable differences among lakes throughout the globe and a paucity of adequate measurements, especially in tropical regions, lead to uncertainty in empirical estimates and in validation of models of methane fluxes. Key processes producing and consuming methane and factors controlling emissions are known, and have been examined in laboratory and field experiments and through statistical analyses (e.g., Bridgham et al., 2013; DelSontro et al., 2016; Harrison et al., 2021; Knox et al., 2021; Segers, 1998). However, interactions

Investigation: John M. Melack, Pedro M. Barbosa, Joao H. F. Amaral
Methodology: Mingyang Guo, John M. Melack, Wencai Zhou
Project Administration: John M. Melack, Qianlai Zhuang
Resources: John M. Melack
Software: Mingyang Guo, Wencai Zhou
Supervision: John M. Melack, Qianlai Zhuang
Validation: Mingyang Guo, Wencai Zhou
Visualization: John M. Melack, Wencai Zhou
Writing – original draft: Mingyang Guo, John M. Melack
Writing – review & editing: Mingyang Guo, John M. Melack, Wencai Zhou, Pedro M. Barbosa, Joao H. F. Amaral, Qianlai Zhuang

among the processes under the wide range of ecological conditions in lakes are not sufficiently understood. The combination of mechanistic models with results from intensive field data provides one way to improve understanding of the processes and sources of variability.

Lakes and associated wetlands cover extensive areas in northern latitudes and in tropical regions (Melton et al., 2013; Messager et al., 2016; Pekel et al., 2016) and represent major sources of methane to the atmosphere (Kirschke et al., 2013; Peng et al., 2022; Rosentreter et al., 2021; Saunois et al., 2020). Riverine floodplains constitute extensive aquatic ecosystems in the tropics and are characterized by seasonal floods that promote the exchange of nutrients and organisms among habitats and substantial primary production (Junk, 1997). For example, floodplains, lakes, and other wetlands cover approximately 1 million km^2 of the Amazon basin (Hess et al., 2015; Sippel et al., 1991). Due to the large area and abundant carbon supplies, these aquatic habitats are important methane sources to the atmosphere (Barbosa et al., 2020; Basso et al., 2021; Beck et al., 2012; Melack et al., 2004; Pangala et al., 2017). However, large uncertainties persist in estimates of tropical CH_4 emission, largely due to the few studies at appropriate temporal and spatial scales. Most field measurements in the Amazon basin and elsewhere in the tropics do not sufficiently capture diel and seasonal variations and often include diffusive, but not ebullitive, methane fluxes.

While temperate and arctic lakes undergo strong seasonal variations in solar radiation and temperature, tropical lakes typically have muted seasonal variations in climate but undergo diel cycles of stratification and mixing (MacIntyre & Melack, 2009; Talling & Lemoalle, 1998). Floodplain lakes have additional biogeochemical and ecological variability caused by changes in water level, connectivity to rivers and optical properties (Melack et al., 2009, 2021). Despite the importance of floodplains with shallow lakes and variable water levels, existing biogeochemical models of methane fluxes are not designed for these environments.

Most current biogeochemical ecosystem models of methane emissions are focused on wetlands, not lakes, and do not include most mechanisms influencing methane emissions (e.g., Bloom et al., 2017; Nzotungicimpaye et al., 2021; Ringeval et al., 2014). Potter et al. (2014) proposed a model for Amazon floodplains based on the supply of organic carbon as a key factor determining methane production. The model requires estimates of carbon inputs, uses simple statistical relations for physical processes, and was evaluated at one lake. The LAKE model (Stepanenko et al., 2016) includes most key processes, but the methane module has only been tested in a small boreal lake, and several physical processes use formulations not well suited to shallow tropical waters.

The Arctic Lake Biogeochemical Model (ALBM) is a one-dimensional (1-D) process-based, biogeochemical model that simulates the thermal and carbon dynamics of lakes (Tan et al., 2015, 2017). The model has been applied to arctic and boreal lakes on seasonal time scales (Guo et al., 2020; Tan et al., 2015), but the thermal module and several other aspects are not appropriate for conditions in shallow, warm waters. In particular, the daily cycles of stratification and mixing and intense, near-surface stratification, that can enhance gas exchange, are not modeled by ALBM. Shallow, warm lakes often develop strong gradients and large variations in dissolved oxygen, that influence methane production and oxidation, and modeling these conditions over diel cycles is required.

In this study, we modified ALBM and combined it with a 3-dimensional (3-D) hydrodynamic model (AEM3D) suited to tropical floodplain lakes and similar shallow, warm waters. The combined model performances in simulating methane processes and fluxes were evaluated in a representative central Amazon floodplain lake with observations of meteorological variables, water temperatures and limnological conditions, and methane diffusive and ebullitive emissions over the seasonal hydrological phases with large differences in water levels (Barbosa et al., 2020, 2021). Our aim is to build a biogeochemical model that reasonably represents individual processes in Amazon floodplain lakes, and other shallow warm waters, and provides methane fluxes at multiple time scales. To do so, we incorporated algorithms for methane and dissolved oxygen production and consumption and selected and calibrated rate functions and coefficients appropriate for ecological conditions in shallow warm-water lakes. To include physical processes that generate diel variations in mixing we used outputs from a 3-D hydrodynamic model and added improved mechanistic understanding of gas exchange.

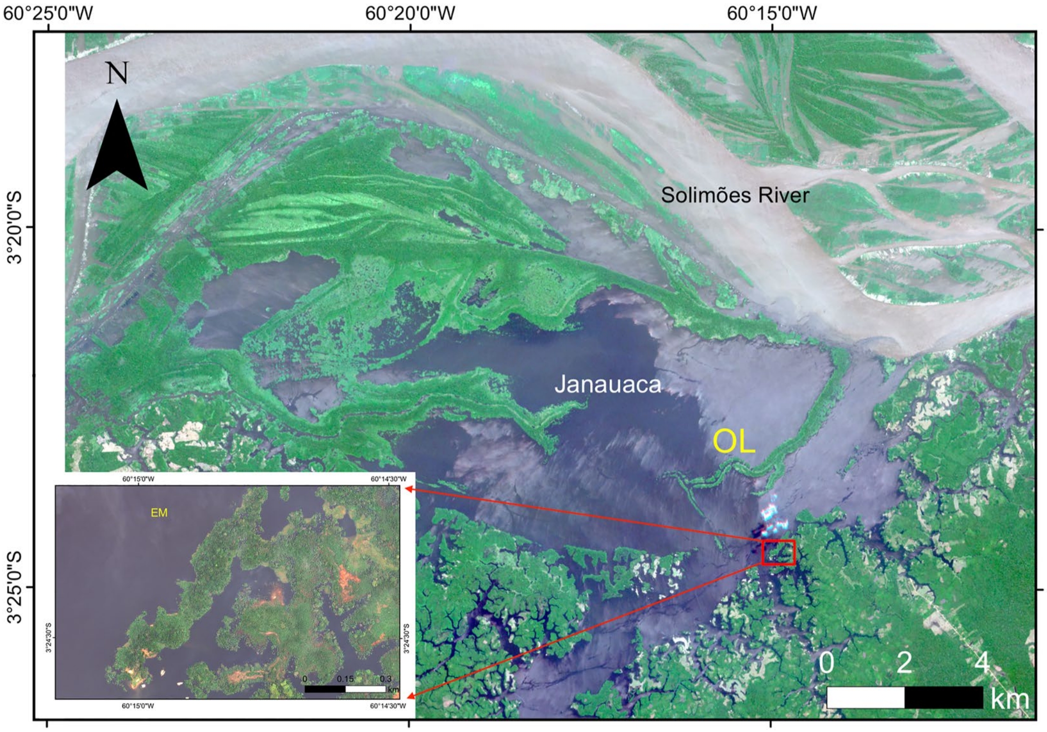

Figure 1. Janauacá floodplain on southern side of Solimões River in central Amazon basin. OL marks approximate location of sampling site in open water of lake. Red box marks location of embayment with an enlarged image of the embayment (EM) shown in the insert. Planet Scope Rapid-eye image acquired on 15 August 2015 with spatial resolution of 6.5 m resampled to a 5-m grid. Insert is an Apollo WorldView-2 image acquired on 14 August 2014 with 0.7 m resolution.

2. Methods

2.1. Study Sites and Measurements

Lake Janauacá is a large floodplain lake in the central Amazon basin connected to the Solimões River (3.38°S, 60.25°W; Figure 1). The lake and associated environments represent ecological and hydrological conditions on central Amazon floodplains, as summarized in Melack et al. (2009) and Melack (2016), and therefore, serves well as a site at which to develop and test a methane model. Measurements were made in the main lake and an embayment from August 2014 to September 2016; a subset of these data were used to develop, calibrate and evaluate the model (Table 1, Figure 2). The lake is fringed by flooded forests and floating herbaceous plants during a portion of the year. The wide range of water depths, surface areas and light attenuation and two sites, though typical of floodplain lakes, could be considered examples of different types of lakes.

The seasonal range of chlorophyll-a (Chla) (2.8–50.5 $\mu g\ L^{-1}$), total phosphorus (1.9–3.8 $\mu mol\ L^{-1}$) and total nitrogen (21–108 $\mu mol\ L^{-1}$) in Lake Janauacá indicate mesotrophic conditions during high water and eutrophic conditions during low and rising water (Melack et al., 2021). Dissolved organic carbon is moderately high (2.5–6.6 $mg\ L^{-1}$), and total suspended solids varied seasonally from up to 115 $mg\ L^{-1}$ during low and rising water to 2.4 $mg\ L^{-1}$ during high water (Melack et al., 2021).

During each field campaign, environmental variables were measured at each site and fringing habitats over 24-hr periods (Barbosa et al., 2020). Water temperatures and dissolved oxygen (DO) concentrations were manually measured every 0.5 m using temperature and oxygen probes and using thermistors and optical DO sensors deployed on moorings at multiple depths. Diffusive methane fluxes were measured with floating chambers and repeated at least three times a day in all habitats. Ebullitive fluxes were obtained using bubble traps. Concentrations of Chla were determined spectrophotometrically using filtered water samples. Detailed methods are described in Barbosa et al. (2020, 2021).

Water levels were recorded daily at stage gauges; a digital elevation model of bathymetry is based on Pinel et al. (2015). Shielded air temperature and relative humidity, solar radiation, wind speed and wind direction,

Table 1

Site, Measurement Date, Surface Area (km^2), Maximum Depth (m), and Hydrological Phase: Rising Water, RW; High Water HW; Falling Water, FW; Low Water, LW

Calibration										
Site	Main lake					Embayment				
Year	2015	2015	2015	2016	2016	2015	2015	2015	2016	2016
Month	Mar	Jun	Oct	Jan	Aug	Feb	Jun	Oct	Jan	Aug
Area	53.1	53.5	16.7	41.3	53.1	0.15	0.17	0.04	0.09	0.17
Depth	7.0	10.7	1.9	3.5	6.8	6.1	11.7	1.0	2.8	6.2
Phase	RW	HW	LW	RW	FW	RW	HW	LW	RW	FW
Validation										
Site	Main lake					Embayment				
Year	2015	2015	2015	2016	2016	2015	2015	2015	2016	2016
Month	Jan	May	Aug	Feb	Apr	Jan	May	Aug	Feb	Apr
Area	50.7	53.4	53.4	42.4	52.3	0.12	0.17	017	0.09	0.16
Depth	6.1	9.8	8.6	3.7	5.7	5.0	11.0	9.5	2.9	6.9
Phase	RW	HW	FW	RW	RW	RW	HW	FW	RW	RW

Note. Calibration refers to periods used to calibrate the model. Validation refers to periods used to test to the model; results for these periods are also referred to as uncalibrated values. Section 2.4 discusses calibration and validation procedures.

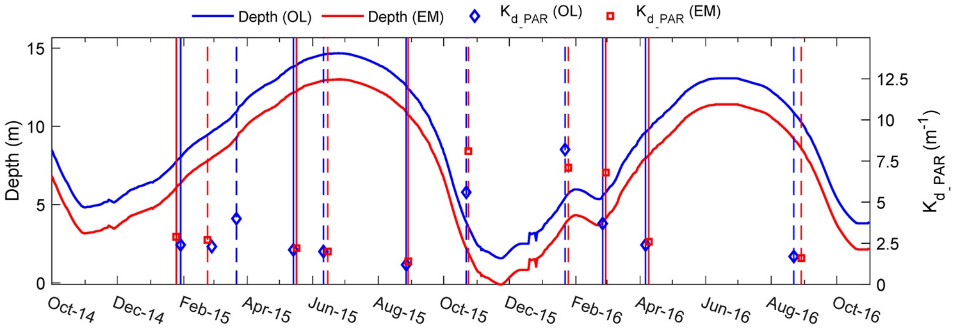

Figure 2. Maximum depths in main lake (OL, blue curve) and embayment (EM, red curve) from October 2014 to November 2016. Attenuation coefficient of PAR (K_{d_PAR}) in OL (blue diamonds) and EM (red squares). Blue and red dashed lines mark the periods when AEM3D and ALBM calibration simulations were done, and blue and red solid lines mark the periods of the validation simulations.

sampled per second and averaged to five-minute intervals, were measured near each site at a floating laboratory. Wind speed and direction sensors were also deployed at 2 m above the water surface at each open water site during field campaigns. Underwater light attenuation over the spectral range from 400 to 700 nm (photosynthetically available radiation, PAR) was measured with a submersible sensor; these data were used to calculate the attenuation coefficient ($K_{d\,\mathrm{PAR}}$).

2.2. Hydrodynamic Model

The hydrodynamic portion of the 3-D Aquatic Ecosystem Model (AEM3D; Hodges & Dallimore, 2019) was used to model thermal structure, mixing and turbulent energy dissipation. AEM3D is derived from the Estuary, Lake and Coastal Ocean Model (Hodges et al., 2000) and uses a z-coordinate Cartesian grid allowing non-uniform spacing in three directions and solves the unsteady Reynolds-averaged Navier-Stokes equation under the Boussinesq approximation. The model adopts a numerical scheme modified from TRIM-3D (Casulli & Cheng, 1992) and simulates temperature with the ULTIMATE-QUICKEST method for scalar transport (Leonard, 1991). Details about the AEM3D numerical schemes are provided by Hodges (2000). The model was run with a 30 s time-step, 100 m × 100 m × 0.1 m grid in the main lake and a 20 s time-step, 5 m × 5 m × 0.1 m grid in the embayment. It was configured with 150 and 130 Eulerian layers for the main lake and the embayment, respectively; the number of layers is the water depth divided by the vertical resolution and changes with water level. Initial conditions include temperature and salinity profiles. Initial temperature profiles were obtained from temperature measurements at the open water sites at mid-night when the water column was mixed or weakly stratified. Initial salinity profiles were estimated from specific conductivity data. Bulk transfer coefficients for heat and momentum were initialized with values for neutral atmospheric stability, which were updated at each time step taking into account the effects of non-neutral atmospheric stability. Bathymetric, meteorological and water level data, described in Section 2.1, are used as inputs to the model.

Vertical mixing is simulated using the mixed-layer model adopted from a 1-D hydrodynamic model (Imberger & Patterson, 1981; Spigel et al., 1986), in which the rate of turbulent kinetic energy (TKE) dissipated (denoted epsilon, ε) is computed as follows: (a) The model calculates the generation of TKE by wind at the surface, drag at bottom and shear in the interior of the water column. (b) The model calculates the energy required to completely mix two adjacent layers at each depth, if stable thermal structure is detected, or TKE generated by convection, if unstable thermal structure is detected. (c) The model conducts full mixing, partial mixing or no mixing depending on the amount of TKE generated compared to the amount of potential energy that needs to be overcome. (d) The amount of TKE to be dissipated is calculated as a function of the simulation timestep, layer thickness and TKE remaining after mixing is conducted, but limited to 100% of the TKE remaining. The TKE dissipation rate is then computed by dividing the amount of TKE dissipated by the simulation time step.

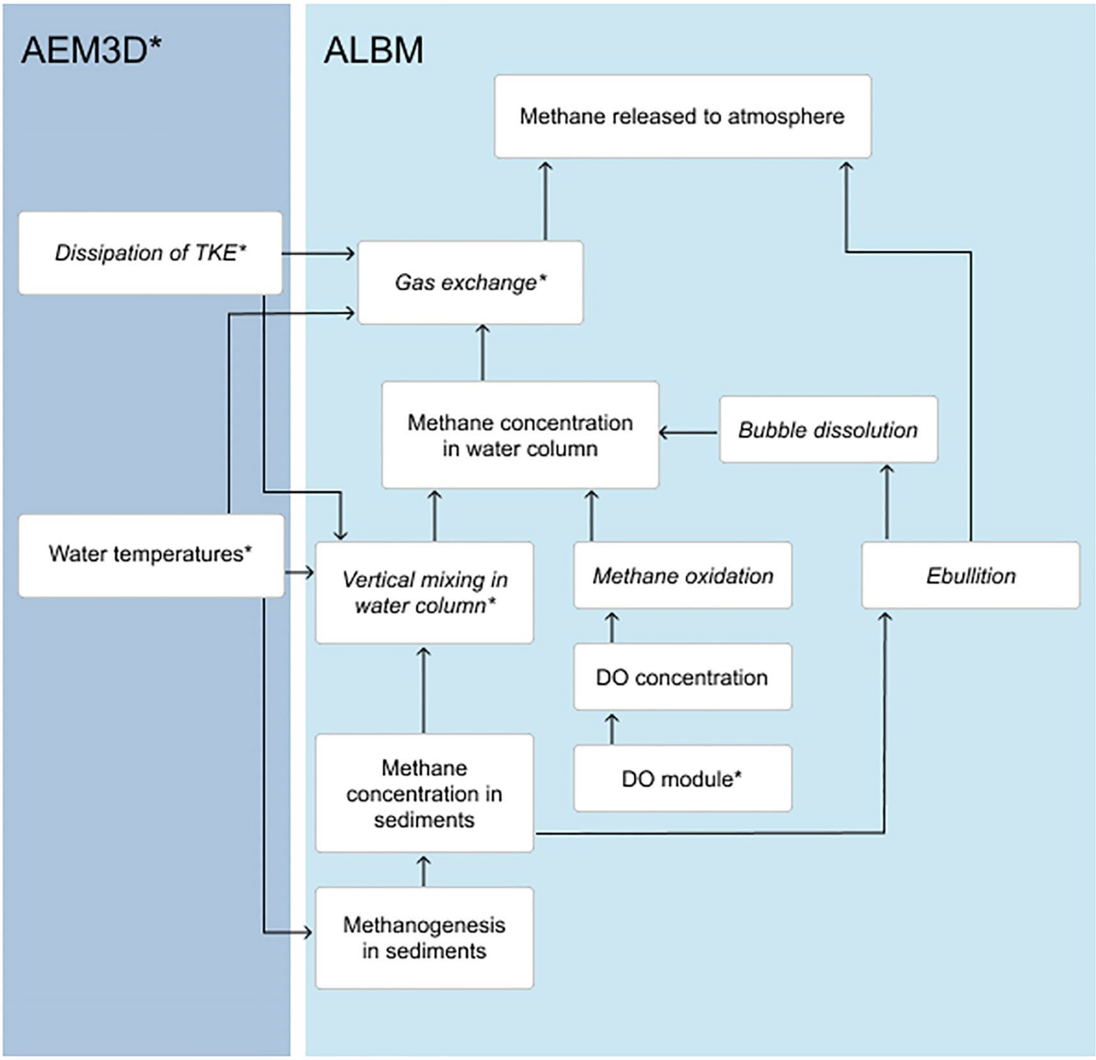

Figure 3. Processes and fluxes modeled in ALBM and supplied by AEM3D. Items marked with an asterisk are new features compared to the prior version of ALBM. Items in italics are rates or fluxes, and those not in italics are quantities. Refer to the Methods for equations and explanations of items shown.

2.3. Biogeochemical Model

We made several modifications to the Arctic Lake Biogeochemical Model (ALBM, Tan et al., 2015, 2017; Guo et al., 2020) to suit Amazon floodplain lakes (illustrated in Figure 3). The thermal module in ALBM was not used, and hydrodynamic inputs (water temperature and ε) were obtained from AEM3D. The Hostetler-based algorithm used in the original ALBM computes eddy diffusivity (K_z) as a function of the latitudinal Ekman profile, 2-m wind speed, and the buoyancy frequency induced by the density gradient (Hostetler & Bartlein, 1990), and does not produce correct values in the shallow warm-waters of Amazon floodplain lakes. The Hostetler-based algorithm produces low K_z with high N values as it assumes that turbulent mixing is suppressed by stratification. This is not the case in shallow tropical waters where the buoyancy frequency in upper water column during diurnal stratification can reach up to 120 cycles per hour (indicating strong stratification), while active mixing is observed (MacIntyre et al., 2021). In contrast, at deeper depths Hostetler-based algorithm-based eddy diffusivities are too large, mixing dissolved gas too fast, and do not match observations.

The modified ALBM uses vertical profiles of water temperatures provided by AEM3D at five-minute time steps. The water column in AEM3D is gridded with 0.1-m intervals, and ALBM is discretized vertically with the same intervals. The mixing depth is assumed to be the depth at which the water temperature is 0.05°C lower than the temperature at 0.05 m. We used ε and thermal structure modeled by AEM3D to estimate vertical mixing, K_z, and

Table 2
Values, Units, and Sources of Parameters in the Formulations of Methane and Oxygen Processes

Fixed-valued parameters

Parameter symbol	Value	Unit	Source
$\boldsymbol{K_m}$	$1.4 \cdot 10^{-7}$	$m^2 s^{-1}$	Subin et al. (2012)
$\boldsymbol{T_{p0}}$	3.5	°C	Walter and Heimann (2000), Marotta et al. (2014)
$\boldsymbol{OQ_{10}}$	1.13	–	Guo et al. (2020)[a]
$\boldsymbol{T_{O0}}$	30	°C	Barbosa et al. (2018)[b]
$\boldsymbol{k_{CH_4}}$	$1.41 \cdot 10^{4}$	μmolm^{-3}	Segers (1998)
$\boldsymbol{k_{O_2}}$	$7.8 \cdot 10^{4}$	μmolm^{-3}	Guo et al. (2020)[a]
$\boldsymbol{K_2}$	$4.2 \cdot 10^{-3}$	molm$^{-2}s^{-1}$	Megard et al. (1984)[c]
$\boldsymbol{\theta_r}$	1.045	–	Ambrose (1988)[c]
$\boldsymbol{\theta_p}$	1.025	–	Stefan and Fang (1994)[c]
$\boldsymbol{\theta_s}$	1.065	–	Stefan and Fang (1994)[c]

Calibrated parameters

Parameter symbol	Value range	Unit	Source
$\boldsymbol{Rc}$	$[9.6 \cdot 10^{-3}, 4.8 \cdot 10^{-1}]$	μmolm$^{-2}s^{-1}$	Gudasz et al. (2010)
$\boldsymbol{\alpha_z}$	[1,10]	–	Stepanenko et al. (2016)
$\boldsymbol{PQ_{10}}$	[0.9,17]	–	Duc et al. (2010), Inglett et al. (2012); Walter and Heimann (2000)[d]
$\boldsymbol{\alpha_e}$	[0.2,1.0]	–	Baird et al. (2004)[e]
$\boldsymbol{O_{max}}$	$[9.6 \cdot 10^{-4}, 3.73]$	μmolm^{-3}s^{-1}	Barbosa et al. (2018)
$\boldsymbol{Ph_{max}}$	$[6.39 \cdot 10^{-4}, 3.09 \cdot 10^{-2}]$	mgO$_2$(mgChla)$^{-1}$s^{-1}	Forsberg et al. (2017)
$\boldsymbol{R_r}$	$[4.94 \cdot 10^{-4}, 4.7 \cdot 10^{-3}]$	mgO$_2$(mgChla)$^{-1}$s^{-1}	Amaral et al. (2018)[f]
$\boldsymbol{k_s}$	$[1.74 \cdot 10^{-2}, 1.15 \cdot 10^{-1}]$	mgO$_2$m^{-2}s^{-1}	Stefan and Fang (1994)[c]

Note. Parameters with empirical values are listed with the values and those calibrated are listed with ranges.

[a]Calibrated values from previous study on boreal lake modeling used. [b]Daily mean water temperature of the sampled lake is used. [c]The K_2, θ_r, and θ_s values fitted to experimental data under temperatures >10°C are used. Measured k_s values for eutrophic lakes with nutrient-rich sediment are used. [d]The PQ_{10} range obtained from observed values in northern wetlands, subtropical wetlands, and boreal and northern temperate lakes with sediments incubated from 0 to 35°C. [e]Bubble formation was found to be activated in two poorly decomposed near-surface bog peats at methane concentrations as low as 20% of the saturation level. [f]Community respiration rates and Chl-a concentrations measured in Lake Janauacá at different times through the year. The Chl-a specific respiration rates are calculated by division.

to distribute the dissolved gases. The gas transfer velocity was modified to a TKE dissipation-based algorithm (MacIntyre et al., 2019). Manually measured DO concentrations at the beginning of the simulation periods were used as initial conditions. A spin-up period of 90 days was used for each hydrological period by repeatedly using representative 24-hr temperatures and turbulence dissipation (from AED3D) and measured dissolved oxygen to numerically stabilize water column methane concentrations before running transient simulations. AEM3D does not require spin-up.

Photosynthesis and metabolism algorithms were simplified by using measured Chla concentrations and Chla-specific process rates. Values of default parameters (Table 2) were adjusted to ranges expected in the Amazon basin. Sediment oxygen demand was added to the model. The revised algorithms and formulations of methane and oxygen processes are introduced below. Parameter values and sources are summarized in Table 2; modeled and physical variables, parameters and coefficients are listed in Table 2 and Appendix A with units.

Methanogenesis in the sediment (P) is modeled as

$$P = R_c \cdot PQ_{10}^{\frac{T_s - T_{P0}}{10}} \cdot e^{-\alpha_z z_s} \tag{1}$$

where R_c is the carbon mineralization rate, PQ_{10} is a Q_{10} factor, T_s is the sediment temperature, T_{p0} is a reference temperature, z_s is depth in sediment; production decreases exponentially with sediment depth at rate α_z. We do not differentiate the sediment carbon between the fraction utilized for methane production and other processes based on the assumption that the carbon supply does not limit methane production. This is a reasonable assumption based the large carbon inputs from herbaceous plants, litterfall from trees and inflows from river and streams to Amazon floodplain lakes (Melack & Engle, 2010). Sediments in Amazon floodplains generally have moderate to high organic carbon content (Moreira-Turcq et al., 2013; Smith et al., 2003; Sobrinho et al., 2016). Sediment temperature was initialized with the annual mean near-bottom water temperature and then simulated based on heat conduction in water and sediments (Tan et al., 2015).

Methane concentrations ($C_{CH_4 s}$) and vertical transfer in the sediment is simulated by

$$\frac{\partial C_{CH_4 s}}{\partial t} = \frac{\partial}{\partial z}\left(K_{ms}\frac{\partial C_{CH_4 s}}{\partial z}\right) + P - \alpha_{CH_4} E_s \tag{2}$$

where K_{ms} is molecular diffusivity in sediment, α_{CH_4} is the percentage of methane in bubbles, and E_s is ebullition. Bubbles consist of nitrogen and methane, and their formation is activated when sediment methane concentrations reach a saturation level, α_e, which is calibrated. The initial bubble diameters are assumed to range between 5 and 20 mm with a uniform distribution of surface tension at the water-sediment interface.

Methane is transported through the water column by eddy diffusivity, entrainment, and ebullition. The changes in methane concentrations ($C_{CH_4 w}$) in the water column are calculated as

$$\frac{\partial C_{CH_4 w}}{\partial t} = \frac{\partial}{\partial z}\left((K_z + K_m)\frac{\partial C_{CH_4 w}}{\partial z}\right) - O + E_{CH_4 w} + F_{met} + P \tag{3}$$

where K_z is eddy diffusivity, K_m is molecular diffusivity, O is aerobic methane oxidation, $E_{CH_4,w}$ is the gas exchange with bubbles, F_{met} is diffusive methane flux at the water-air interface, and P is methanogenesis in the sediment. Methane exchanges at the sediment-water and water-air interfaces are added to the bottom and top boundaries, respectively. Advection from fringing habitats may also change methane concentrations, as mentioned in the Discussion, but are not included in the 1-D structure of ALBM. Eddy diffusivity is calculated as $K_z = 0.2\varepsilon/N^2$, where 0.2 is Osborne coefficient, ε is the TKE dissipation rate, and $N = \sqrt{-\frac{g}{\rho}\frac{\partial\rho}{\partial z}}$ is the Brunt-Väisälä frequency, and ρ is water density. Water columns with $N < 10^{-2}\ s^{-1}$ are treated as well-mixed, and the gas concentrations are simulated as the volume-weighted mean.

Aerobic methane oxidation is a function of water temperature, and methane and dissolved oxygen concentrations following Segers (1998) and Zhuang et al. (2004):

$$O = O_{\max} \cdot OQ_{10}^{\frac{T_w - T_{O0}}{10}} \frac{C_{O_2}}{k_{O_2} + C_{O_2}} \frac{C_{CH_4,w}}{k_{CH_4} + C_{CH_4,w}} \tag{4}$$

where $O_{\max}$ is methane oxidation potential, OQ_{10} is a Q_{10} factor, T_w is water temperature, T_{O0} is a reference temperature, and k_{O_2} and k_{CH_4} are Michaelis-Menten constants.

The governing equations of bubble transfer in the water column are adapted from ocean models (Liang et al., 2011; Woolf & Thorpe, 1991). The gas concentration in bubbles of certain size at certain depth and time step is calculated by a continuity equation in which the impacts of buoyant rising, gas exchange with ambient water, and bubble expansion are included (Liang et al., 2011). Buoyant rising is driven by the hydrostatic pressure gradient across the water columns and kinematic viscosity, and gas exchange by the pressure difference between in- and outside of the bubble. The size of a single bubble changes during rising depending on the air pressure, hydrostatic pressure, and bubble surface tension. Gases in bubbles are assumed to release instantly to the atmosphere upon reaching the lake surface. Detailed formulations can be found in Tan et al. (2015).

The dissolved oxygen module is based on Stefan and Fang (1994) with modifications to suit the availability of observational data. The changes in concentrations of dissolved oxygen $\left(C_{O_2}\right)$ in the water column are modeled as

$$\frac{\partial C_{O_2}}{\partial t} = \frac{\partial}{\partial z}\left((K_z + K_m)\frac{\partial C_{O_2}}{\partial z}\right) + Ph - R - SOD - 2 \cdot O + F_{ox}\mathrm{g} \tag{5}$$

Table 3
Calibrated Parameter Values for Main Lake

Parameter	Units	201503	201506	201510	201601	201609
$\boldsymbol{Rc}$	μmol$m^{-2}s^{-1}$	$2.33 \cdot 10^{-2}$	$3.07 \cdot 10^{-2}$	$2.05 \cdot 10^{-2}$	$5.5 \cdot 10^{-2}$	$1.71 \cdot 10^{-2}$
$\boldsymbol{\alpha_z}$	–	4.54	3.0	3.50	4.36	5.64
$\boldsymbol{PQ}10$	–	1.84	2.64	5.99	7.61	1.77
$\boldsymbol{\alpha_e}$	–	0.41	0.45	0.86	0.64	0.63
$\boldsymbol{O_{max}}$	μmol$m^{-3}s^{-1}$	$1.26 \cdot 10^{-2}$	$2.52 \cdot 10^{-3}$	$2.33 \cdot 10^{-2}$	$5.56 \cdot 10^{-3}$	$4.43 \cdot 10^{-2}$
$\boldsymbol{Ph_{max}}$	$mgO_2(mgChla)^{-1}s^{-1}$	$1.08 \cdot 10^{-2}$	$7.76 \cdot 10^{-3}$	$3.55 \cdot 10^{-2}$	$7.96 \cdot 10^{-3}$	$1.15 \cdot 10^{-2}$
$\boldsymbol{R_r}$	$mgO_2(mgChla)^{-1}s^{-1}$	$2.54 \cdot 10^{-3}$	$4.5 \cdot 10^{-3}$	$1.96 \cdot 10^{-3}$	$3.37 \cdot 10^{-3}$	$4.45 \cdot 10^{-3}$
$\boldsymbol{k_s}$	$mgO_2m^{-2}s^{-1}$	$7.32 \cdot 10^{-2}$	$8.94 \cdot 10^{-2}$	$1.27 \cdot 10^{-2}$	$3.22 \cdot 10^{-2}$	$1.84 \cdot 10^{-2}$

where Ph is oxygen production by photosynthesis, R is community respiration, SOD is sediment oxygen demand, O is aerobic methane oxidation and F_{oxg} is oxygen exchange at the air-water interface. Photosynthetic rate is computed as $\mathrm{Ph} = \mathrm{Ph}_{\max}\theta_p^{T_w-30}\mathrm{f}(I, T_w)C_{\mathrm{Chla}}$, where $\mathrm{Ph}_{\max}$ is the Chla-specific light-saturation rate of photosynthesis, θ_p is a temperature coefficient estimated as a function of optimal temperature, standard temperature, and maximum temperature from model input data (Tan et al., 2017), $f(I,T_w)$ is a light limitation term, I is the incident photosynthetically active radiation, and C_{Chla} is Chla concentration. $f(I, T_w) = I\left(1 + 2\sqrt{K_1/K_2}\right)/\left(I + K_1 + I^2/K_2\right)$, where K_1 $\left(\text{approximated as } 0.7 \times 1.1^{T_w-20}\right)$ and K_2 are light inhibition and limitation coefficients. Respiration rate depends on temperature and Chla: $R = R_r\theta_r^{(T_w-30)}C_{Chla}$, where R_r is the Chla-specific respiration rate at 30°C, and θ_r is a temperature coefficient. The vertical distribution of Chla is assumed uniform, though only involved in photosynthesis within the euphotic zone. The euphotic zone is delimited by the depth where PAR was more than 1 μmolm^{-2} s^{-1}, a value selected because the phytoplankton are circulating in turbid water. SOD is a function of temperature and bathymetry: $\mathrm{SOD} = \frac{k_s\theta_s^{T_w-20}}{A}\frac{\partial A}{\partial z}$, where k_s is the sediment oxygen demand at 20°C, θ_s is a temperature coefficient, and A is sediment area as a function of depth based on the hypsographic curve of depth versus area derived from the lake's bathymetry. As the water level varies seasonally, the appropriate portion of the hypsographic curve is used. If the sediments are overlain by anoxic water, the SOD is zero. Advection between habitats is not included.

Diffusive gas flux at the water-air interface (F) is calculated following $F = k_{600} \cdot (C_w - C_{eq})$, where k_{600} is gas transfer velocity normalized to CO_2 at 20°C, C_w is near-surface gas concentration, and C_{eq} is near-surface gas concentration in equilibrium with the atmosphere. Gas transfer velocity is based on MacIntyre et al. (2019): $k_{600} = c_1(\varepsilon v)^{0.25}Sc^{-0.5}$, where $c_1 = 0.5$ is a constant coefficient, ε is the dissipation rate of TKE at water surface, v is kinematic viscosity, and Sc is the Schmidt number. F was calculated for both methane and dissolved oxygen.

2.4. Biogeochemical Model Sensitivity Tests, Calibration, and Validation

Parameters for calibration were selected through sensitivity tests using a machine learning-based algorithm, classification and regression trees (CART, Krzywinski & Altman, 2017). The CART method trains a decision tree by recursively partitioning the input data into two subgroups by the value of the explanatory variable at each node. The decision tree can be pruned by adjusting the stopping criteria including the number of iterations and the size of subgroups to achieve the best size of the tree and the lowest misclassification rate. This method has proved adequate and widely used in the inspection of multivariant relationships within large complex data (Choubin et al., 2018; Guo et al., 2020; Rodrigues & de la Riva, 2014). In our study, a tree size of 200 nodes was found optimal using the cross-validation method. For each case, the model was run with a perturbed parameter ensemble (PPE) of size 10,000, and the simulated methane and DO concentrations at lake surface and bottom were used as training data for CART. Data training and sensitivity analysis were done using the *R* package "gbm" (Greenwell et al., 2019). Relative influence percentages are based on Friedman (2001).

The model was calibrated separately for each site and water level using a Bayesian approach in which a uniform distribution was prescribed to all parameters, and Monte-Carlo based calibrations were run more than once by sampling from the posterior distribution obtained from the previous round. The periods for calibration were

Table 4
Calibrated Parameter Values for Embayment

Parameter	Units	201502	201506	201510	201601	201609
Rc	$\mu molm^{-2}s^{-1}$	$4.95 \cdot 10^{-2}$	$4.98 \cdot 10^{-2}$	$3.96 \cdot 10^{-2}$	$5.99 \cdot 10^{-2}$	$2.92 \cdot 10^{-2}$
α_z	–	4.93	2.59	3.09	3.0	4.49
$PQ10$	–	2.9	2.57	9.29	6.97	5.48
α_e	–	0.53	0.99	0.43	0.42	0.52
O_{max}	$\mu molm^{-3}s^{-1}$	$6.68 \cdot 10^{-3}$	$2.19 \cdot 10^{-3}$	$1.28 \cdot 10^{-2}$	$6.19 \cdot 10^{-3}$	$1.9 \cdot 10^{-3}$
Ph_{max}	$mgO_2(mgChla)^{-1}s^{-1}$	$2.2 \cdot 10^{-2}$	$1.51 \cdot 10^{-2}$	$6.89 \cdot 10^{-3}$	$2.54 \cdot 10^{-3}$	$2.33 \cdot 10^{-2}$
R_r	$mgO_2(mgChla)^{-1}s^{-1}$	$9.39 \cdot 10^{-4}$	$4.63 \cdot 10^{-3}$	$3.93 \cdot 10^{-4}$	$4.11 \cdot 10^{-3}$	$1.37 \cdot 10^{-3}$
k_s	$mgO_2m^{-2}s^{-1}$	$3.86 \cdot 10^{-2}$	$6.12 \cdot 10^{-2}$	$5.85 \cdot 10^{-2}$	$1.15 \cdot 10^{-1}$	$3.33 \cdot 10^{-2}$

selected to span the seasonal range of water depths and limnological conditions. The number of the sampling round was case-sensitive and decided by the model performance. The size of the PPE equaled number of parameters multiplied by 1,000 in each round. For methane diffusive fluxes, the simulations were compared to hourly observations while for ebullitive fluxes, daily totals were calculated to compare with the observed daily ebullition collected by bubble traps. Simulated DO concentrations were validated against observations at each observational depth. The optimal parameter values were selected based on the simulation accuracy of both methane fluxes and oxygen concentrations (Tables 3 and 4).

Model validation was done by running simulations for other times using the calibrated parameters. For each site, five additional periods were modeled (Table 1) using calibrated parameters from the period with (a) the same hydrological phase, and (b) the closest lake depth. Simulated methane fluxes and concentration were compared to the measurements to evaluate the model performance. Root-mean-square errors ($\mathrm{RMSE} = \sqrt{\frac{\sum_{i=1}^{n}(S_i - O_i)^2}{n}}$) were calculated for methane diffusive fluxes (μmol m^{-2} hr^{-1}) and near-surface methane concentrations (μmol L^{-1}). S_i is simulated value, O_i is measurement, and n is the number of measurements during each simulated period. Measured and simulated methane fluxes and concentrations were compared in time-series figures. Measured and modeled thermal structure and DO concentrations were evaluated using time-depth diagrams.

3. Results

Results are presented in three complementary sections. First, sensitivities of the simulated concentrations and fluxes to parameters used in the model and their relative importance are presented. Second, the simulated methane concentrations and fluxes are compared to measurements with examples of the four hydrological phases in the main lake and embayment for calibrated and uncalibrated periods. Time-series figures and performance metrics are provided. Third, time-depth diagrams of measured and modeled thermal structure and dissolved oxygen concentrations at high and low water levels are provided. Subsequently, the discussion examines simulations of specific processes to help decipher influences of various factors and the veracity of the simulations.

3.1. Parameter Sensitivities

Parameter sensitivity tests were conducted for high and low water periods in the main lake. The simulated methane concentrations, methane fluxes and DO concentrations are sensitive to 8 parameters and the relative importance (RI) of each parameter is fairly consistent between the two hydrological phases (Table 5). Methane concentrations at near-surface and near-bottom are most sensitive to the carbon mineralization rate (Rc), Q_{10} factors for methanogenesis (PQ_{10}) and oxidation (OQ_{10}), and methane oxidation potential ($O_{\max}$) during both hydrological phases. Diffusive emission is sensitive to the same parameters because it is mainly controlled by near-surface methane concentration. Ebullitive emission is sensitive to methanogenesis-related parameters, and to the decrease of sediment organic carbon with depth and percent saturation of methane concentration, as this initiates bubbling. Near-surface and near-bottom DO concentrations are sensitive to community respiration (R_r), sediment oxygen demand, the Q_{10} factor of methanogenesis, and carbon mineralization rate. Only near-surface DO is sensitive to

Table 5

Relative Importance (RI) for Parameters Tested in the Sensitivity Analysis; Diffusive Flux (dflux) and Ebullitive Flux (efflux)

	Near-surface CH_4		Near-bottom CH_4		dflux		eflux		Surface DO		Bottom DO	
Parameters	201506	201510	201506	201510	201506	201510	201506	201510	201506	201510	201506	201510
OQ_{10}	2.4	1.8	2.5	1.4	2.3	2.3	0	0	2.1	0.8	0.3	1.0
k_{CH_4}	0.8	1.48	14.2	0.4	14.3	1.5	0	0.03	0.3	0	0.04	0
k_{O_2}	0.03	0.03	0.05	0.01	0.03	0.02	0	0	0.07	0.01	0	0
Rc	**23.8**	**22.0**	**23.1**	**22.5**	**23.0**	**21.7**	8.8	8.8	14.6	2.2	9.0	1.7
α_z	0.03	0.1	0.06	0.01	0.06	0.2	**20.0**	19.5	0.03	0	0.07	0
PQ_{10}	**56.7**	**57.3**	**56.7**	**60.1**	**57.2**	**56.6**	**24.2**	**25.9**	**53.6**	7.5	**37.4**	5.9
α_e	0.8	14.3	0.7	0.2	0.8	1.1	**46.7**	**45.5**	0.05	0.03	0	0
O_{max}	14.2	1.0	0.9	0.3	0.9	14.1	0	0	1.8	0.5	0.6	0.8
Ph_{max}	0	0	0	0	0	0	0	0.03	0.4	**34.4**	0.2	2.4
R_r	0.1	0.4	0.1	0.03	0.2	0.5	0	0	1.6	**22.7**	2.2	**38.9**
k_s	0.4	0.8	0.4	15.0	0.5	0.9	0	0.04	**24.9**	**31.9**	**49.9**	**49.2**

Note. Values above 20 are bold.

photosynthesis potential (Ph_{max}) and is more sensitive to photosynthesis potential at low water than at high water, probably due to the higher chlorophyll concentrations at low water. High-water near-surface DO is sensitive to methanogenesis-related parameters and thus methane concentration, indicating that the longer methane diffusion pathway makes methanotrophy an important sink for both methane and oxygen. For consistency, the parameters important for at least one hydrological phase were selected to be calibrated for all sites and time periods.

3.2. Methane Fluxes and Concentrations

Main lake - Simulated methane fluxes and concentrations for calibrated (Table 6) and uncalibrated periods (Table S1 in Supporting Information S1) vary in their similarity to measurements. RMSE values for near-surface CH_4 concentrations ranged from 0.5 to 1.5 μmol L^{-1} for calibrated periods from 0 to 3.7 μmol L^{-1} for uncalibrated periods. RMSE values for CH_4 fluxes ranged from 2.6 to 85 μmol m^{-2} hr^{-1} for calibrated periods from 1.3 to 68 μmol m^{-2} hr^{-1} for uncalibrated periods. Time-series of simulated fluxes for calibrated periods show generally good agreement with measurements in Oct 2015 and Jan 2016 but less agreement in Aug 2016 when simulated values are often higher (Figure 4). During uncalibrated periods, simulated fluxes were similar to measurements except for occasional mismatches (Figure S1 in Supporting Information S1).

Vertical profiles of simulated CH_4 concentrations during high water in Jun 2015 were similar to measurements near mid-night (22:45 hr), but differed considerably at mid-day and sunrise (Figure S2 in Supporting Information S1). Vertical variations were usually lacking during low water (October 2015 and January 2016) in both measurements (except for a couple of times in October 2015) and simulations (Figure S3 in Supporting Information S1).

Table 6

Root-Mean-Square Errors (RMSE) for Simulated Variables During Different Water Levels in Main Lake and Embayment for Calibrated Periods

Site	Main lake				Embayment				
Year	2015	2015	2016	2016	2015	2015	2015	2016	2016
Month	Jun	Oct	Jan	Aug	Feb	Jun	Oct	Jan	Aug
Near-surface CH_4 (μ mol L^{-1})	0.5 (3)	0.5 (11)	1.5 (7)	0.8 (20)	0.6 (5)	2.0 (3)	2.2 (7)	2.8 (7)	2.2 (12)
Diffusive CH_4 flux (μ mol m^{-2} hr^{-1})	2.6 (6)	33 (22)	85 (14)	45 (37)	23 (12)	28 (8)	246 (18)	242 (15)	190 (24)

Note. Number in parenthesis is the number of measurements during each simulated period. Mar 2015 not shown because only one measurement overlapped simulated period.

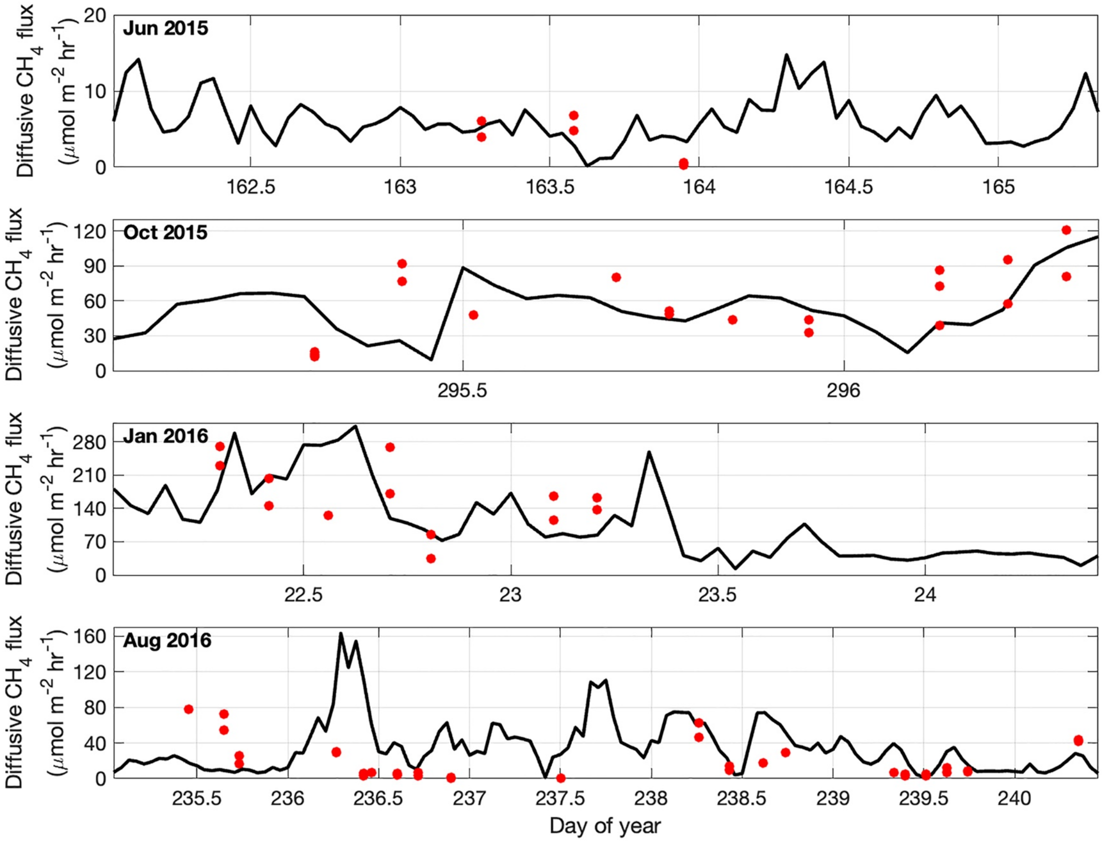

Figure 4. Measured (red dots) and simulated (lines) diffusive fluxes in Lake Janauacá (main lake) for June 2015 (a), October 2015 (b), January 2016 (c), and August 2016 (d). Note different scales on *y*-axes. All replicates of measured fluxes are shown and expressed as hourly values. Simulated diffusive fluxes are summed for each hour and the values are assigned to the end of each hour. Mar 2015 not shown because only one measurement overlapped simulated period.

Table 7
Average Daily Diffusive CH_4 Fluxes (μ mol m^{-2} d^{-1}): ALBM (Calibrated and Uncalibrated) and Measurements

		Main lake				Embayment			
		ALBM		Measurements		ALBM		Measurements	
Simulation dates		S days	Flux (μ mol m^{-2} d^{-1})	n	Flux (μ mol m^{-2} d^{-1})	S days	Flux (μ mol m^{-2} d^{-1})	n	Flux (μ mol m^{-2} d^{-1})
Calibrated	Feb/Mar 2015	1.2	253	4	152	3.3	461	11	482
	Jun 2015	3.3	146	6	90	1.4	250	8	630
	Oct 2015	1.3	1,261	22	1,331	1.3	5,496	8	6,227
	Jan 2016	2.4	2591	14	3,838	1.4	6,931	13	6,495
	Aug 2016	5.5	825	37	497	3.5	3,380	15	2388
Uncalibrated	Jan 2015	2.3	182	12	68	2.9	426	16	365
	May 2015	2.4	37	8	22	2.6	318	8	224
	Aug 2015	1.5	184	8	629	3.4	1,239	8	560
	Feb 2016	2.3	2975	15	1,800	1.3	2445	15	3,221
	Apr 2016	2.5	368	24	275	1.3	2038	24	2431

Note. For ALBM simulations, average diffusive CH_4 fluxes computed as the sum of fluxes divided by the length of simulation, and for measurements as the arithmetic mean of the measurements. Both averages are converted to daily values. S days is number of days simulated; *n* is number of measurements.

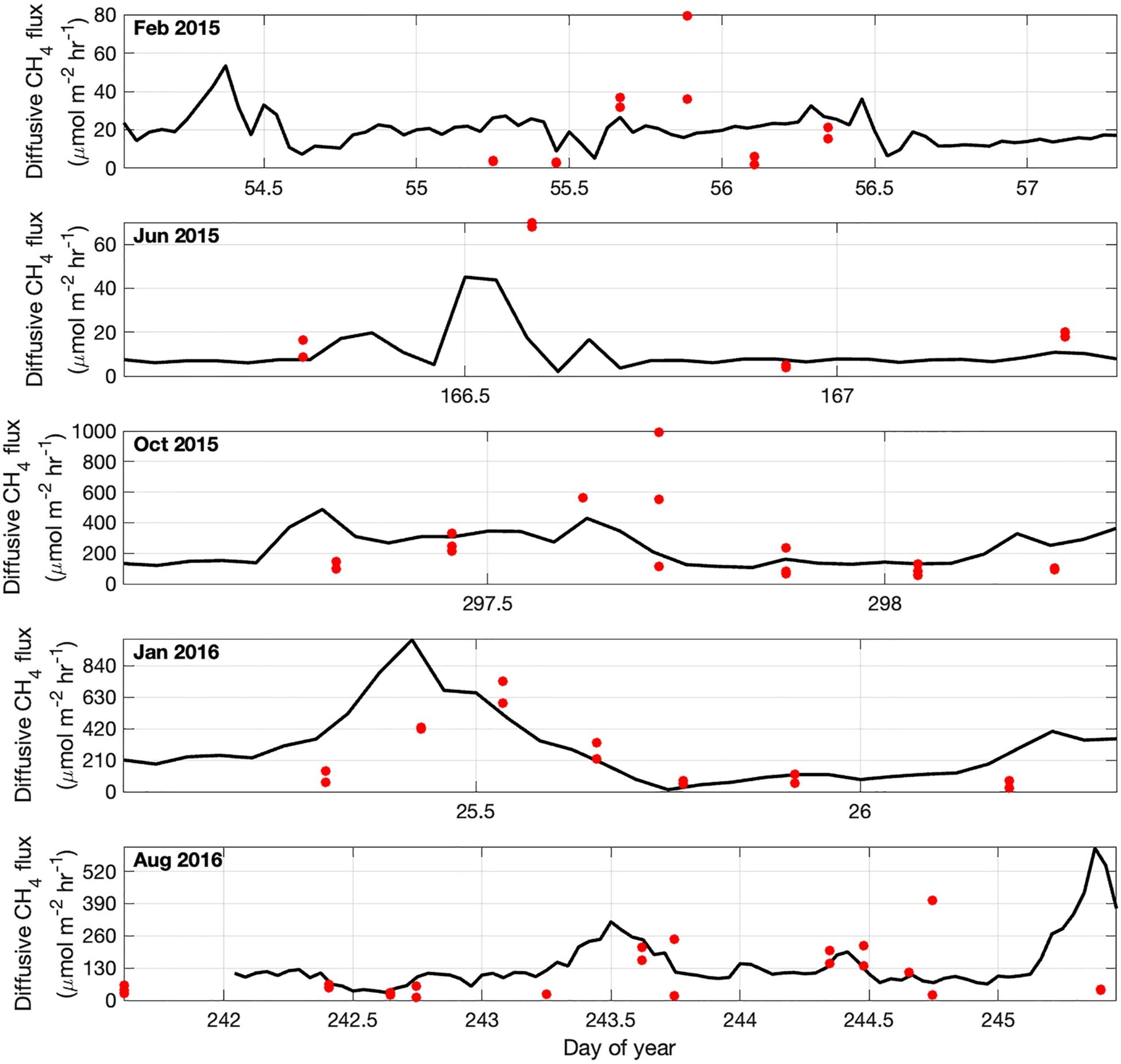

Figure 5. The same as Figure 4 for Lake Janauacá (embayment) in February 2015 (a), June 2015 (b), October 2015 (c), January 2016 (d), and August 2016 (e).

Time-series of simulated near-surface concentrations were consistently less than measurements in Oct 2015 and consistently higher than measurements in Jan and Aug 2016 (Figure S4 in Supporting Information S1). During uncalibrated periods simulated near-surface concentrations matched measurements well in January 2015 and February and April 2016 but less well in May and August 2015 (Figure S5 in Supporting Information S1).

Average daily diffusive CH_4 fluxes, calculated from measurements and simulations, have generally consistent seasonal patterns with higher and lower values matching, albeit with conspicuous differences in August 2016 (calibrated) and August 2015 and February 2016 (uncalibrated (Table 7). The few comparisons available for daily ebullitive fluxes indicate negligible fluxes except during low water (Table S2 in Supporting Information S1).

Embayment—Simulations of methane fluxes and concentrations for calibrated (Figure 5 and Figures S6–S8 in Supporting Information S1; Tables 6 and 7 and Table S2 in Supporting Information S1) and uncalibrated (Table 7, Tables S1 and S2 in Supporting Information S1; Figures S9 and S10 in Supporting Information S1) periods vary in their similarity to measurements. RMSE values for near-surface CH_4 concentrations ranged from 0.6 to 2.8 μmol L^{-1} for calibrated periods from 0.1 to 3.9 μmol L^{-1} for uncalibrated periods. RMSE values for CH_4

fluxes ranged from 23 to 246 μmol m^{-2} hr^{-1} for calibrated periods from 14 to 88 μmol m^{-2} hr^{-1} for uncalibrated periods. Time-series of simulated fluxes for calibrated and uncalibrated periods show generally good agreement with measurements except for occasional mismatches (Figure 5 and Figure S9 in Supporting Information S1).

Vertical profiles of simulated CH_4 concentrations during high water in Jun 2015 were similar to measurements in the upper 2 m, but progressively diverged at deeper depths with simulated values exceeding measurements (Figure S6 in Supporting Information S1). Vertical variations were usually lacking during low water (January 2016) in both measurements (except for a few high values near the bottom) and simulations (Figure S7 in Supporting Information S1). Time-series of simulated near-surface concentrations were consistently more than measurements in August 2016, and comparisons varied in other periods with no patterns (Figures S8 and S10 in Supporting Information S1).

Average daily diffusive CH_4 fluxes, calculated from measurements and simulations, have generally consistent seasonal patterns with higher and lower values matching, albeit with conspicuous differences in August 2016 (calibrated) and August 2015 and February 2016 (uncalibrated (Table S1 in Supporting Information S1). The few data available for daily ebullitive fluxes indicate comparable values and seasonal patterns for measurements and simulations except for a mismatch in values in January 2016 (Table S2 in Supporting Information S1).

An overall comparison of measured and simulated fluxes that combines all replicates of measured diffusive fluxes from both sites and the wide range of water levels and associated ecological conditions indicates considerable variability (Figure S11 in Supporting Information S1), as expected by the results illustrated in figures with measurements and simulated methane fluxes. Temporal variability is not expected to be replicated exactly by ALBM, given the inherent variability of methane fluxes and sparseness of field data.

3.3. Thermal Structure and Dissolved Oxygen Concentrations

The hydrodynamic model simulated well the diurnal stratification and nocturnal mixing in the open lake and embayment during both high and low water periods (Figures 6 and 7). Time-depth plots of simulated and measured DO values for high and low water periods in main lake (Figure 6) and embayment (Figure 7) indicate general similarities in diel and vertical variations. However, in Oct 2015 in the main lake larger day-night differences were simulated than measured (Figures 6b3 and 6b4). RMSE for simulated near-surface dissolved oxygen concentrations (mg L^{-1}) during calibrated periods ranged from 0.9 to 4.4 (Table 8), and for uncalibrated periods from 0.6 to 6.3 (Table S3 in Supporting Information S1). RMSE values for simulated near-bottom dissolved oxygen concentrations (mg L^{-1}) during calibrated periods ranged from 0.1 to 1.4, except for larger values at low water (October 2015); the especially high value in August 2016 is misleading because most of the water column was anoxic. During uncalibrated periods RMSE values from 0.1 to 2.0 mg L^{-1}, except for larger values during low water (January 2015 and February 2016) in the main lake (Table S3 in Supporting Information S1).

4. Discussion

Hipsey et al. (2020) identified several aspects of model performance including comparison of simulated variables with observations, as described in Results, and evaluation of the processes being simulated. Here, we discuss the algorithms used, the basis for revisions of the original ALBM formulations and alternative algorithms for the physical and biogeochemical processes and the inputs needed to apply these algorithms. We compare modeled rates of photosynthesis, respiration and methane oxidation with measurements from Amazon floodplain lakes. We then consider challenges and limitations of modeling methane fluxes including the heuristic value of the model and how the model's result could be used to extend in time and space estimates of methane emissions.

4.1. Algorithms and Processes

4.1.1. Hydrodynamic Models and Inputs

While 3-dimensional hydrodynamic models, such as AEM3D, can characterize most of the relevant physical processes in lakes, these models are computationally demanding. Hence, application of 3-dimensional models to regional analyses over multiple years is not currently practical. One-dimensional hydrodynamic models, such as the "DYnamic REservoir Simulation Model" (DYRESM) and its derivatives (Hipsey et al., 2019; Imberger & Patterson, 1981), also have well characterized parameterizations of physical processes. DYRESM is computationally efficient and has been shown to be accurate with respect to temporal variations in temperature

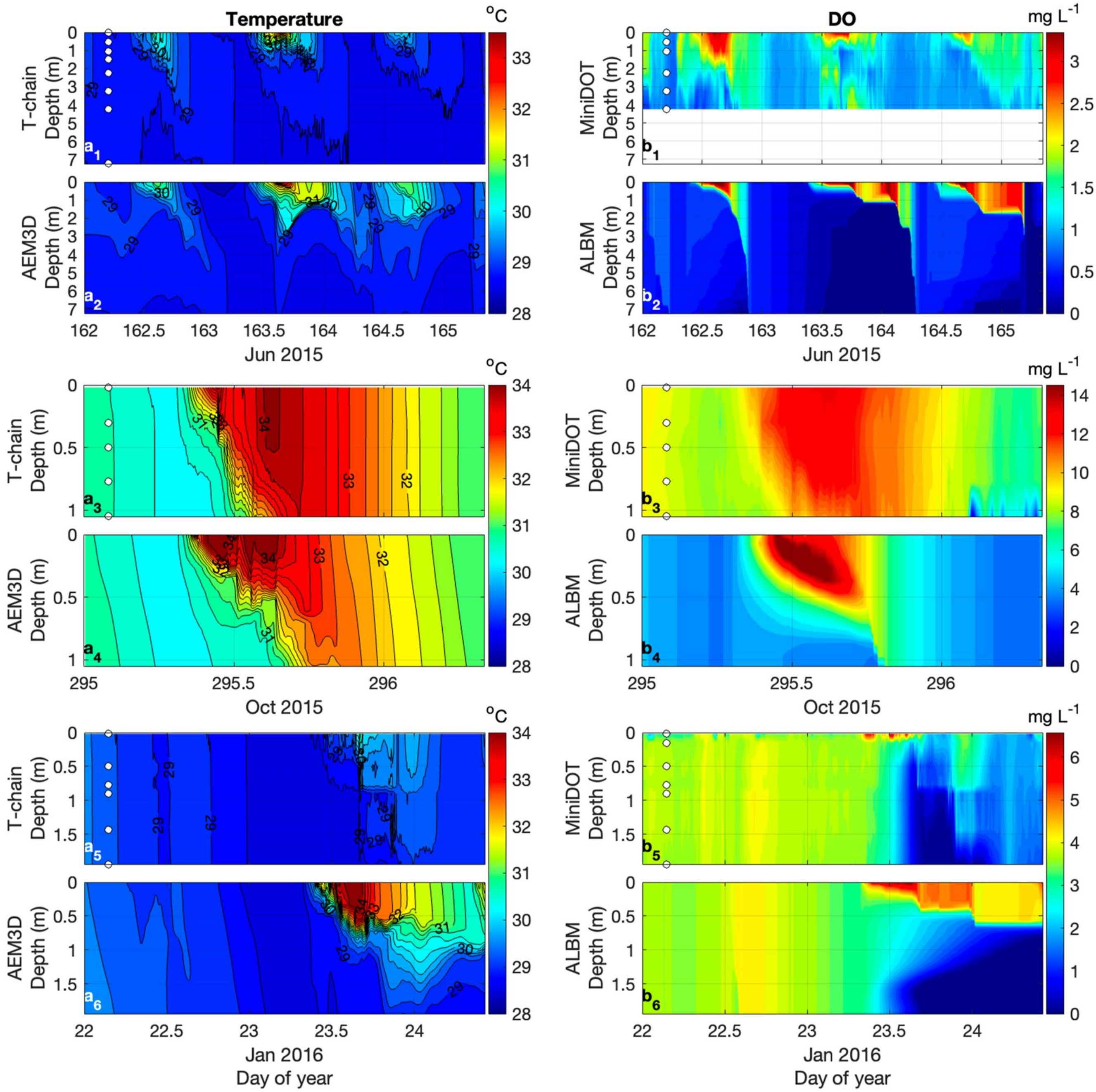

Figure 6. Time-depth plots of measured and simulated temperatures (a_1 to a_6) and dissolved oxygen (DO) concentrations (b_1 to b_6), respectively, during high water (June 2015) and low water (October 2015 and January 2016) in Lake Janauacá (main lake). White dots indicate depths of thermistors or DO sensors. Both the measured and simulated temperatures were averaged with 5-min bins.

structure in seasonally stratified lakes and reservoirs (Yeates & Imberger, 2003). A recent extension to the Multi-Basin DYnamic REservoir Simulation Model (MB-DYRESM) has been developed to bridge between one-dimensional lake models and computationally expensive, three-dimensional lake models (Zhou et al., 2021).

Given the importance of diel variations in physical processes in shallow, warm water lakes, as well as other types of lakes in some seasons, meteorological data at least hourly intervals are required as inputs. Ideally, meteorological sensors are deployed on or near the lake, but meteorological measurements are sparse for Amazon floodplains and seldom on lakes elsewhere. Alternatives for regionalization may be output of the Weather Research and Forecasting model (e.g., Yang & Dominguez, 2019) or reanalysis results, such as the 3-hourly MERRA-2 data at

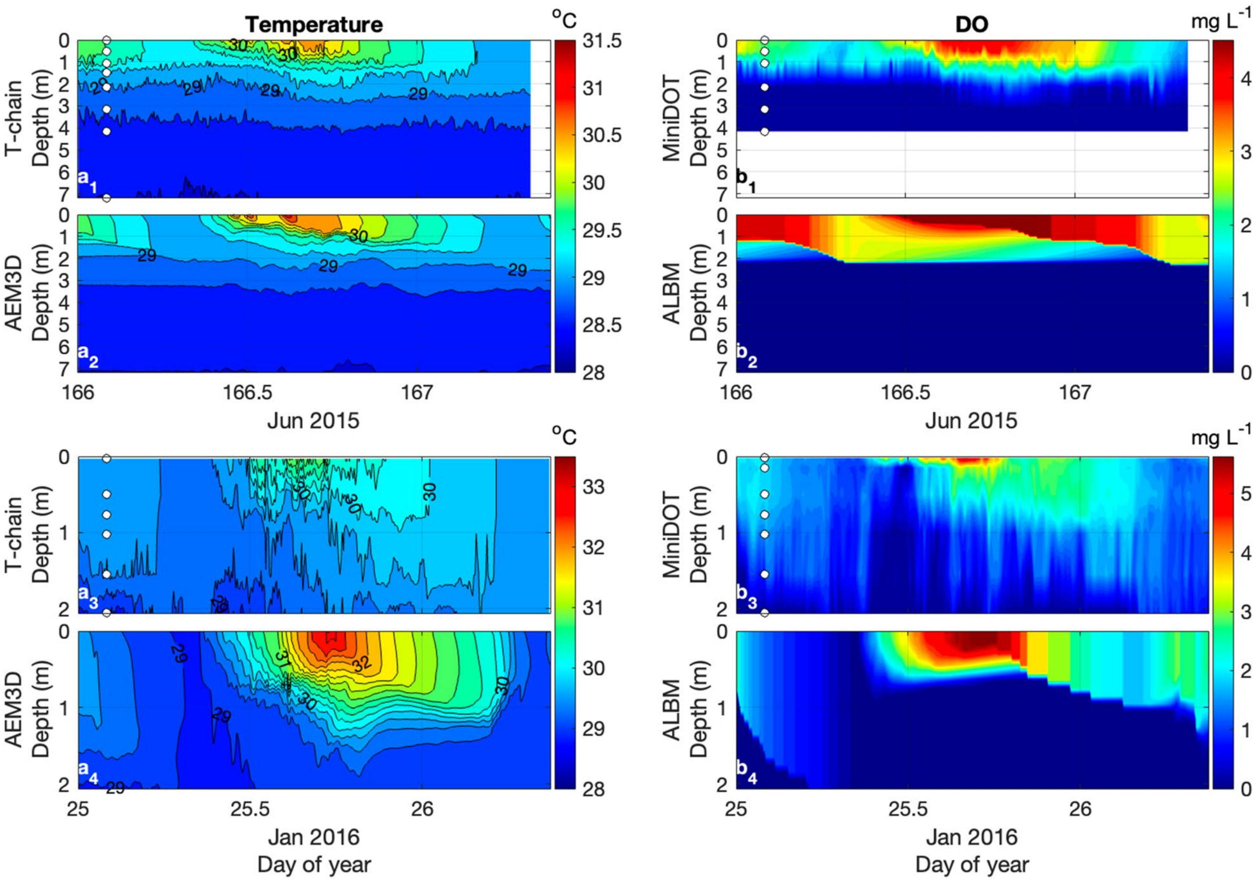

Figure 7. The same as Figure 6 for high water (June 2015) and low water (January 2016) in Lake Janauacá (embayment). White dots indicate depths of thermistors or DO sensors.

0.5° resolution (https://gmao.gsfc.nasa.gov/reanalysis/MERRA-2/), or the ERA5-Land hourly meteorology data at 0.1° (~9 km) resolution (https://doi.org/10.24381/cds.e2161bac). Daily data, such as used for climate projections, are not suitable (e.g., Frieler et al., 2017).

The revised version of ALBM uses a formulation of K_z derived as a TKE-based ε. As an alternative to estimates of TKE by hydrodynamic models, ε can be calculated with meteorological data and thermal structure of the lake, as described in MacIntyre et al. (2019).

Hydrodynamic simulations with AEM3D were done as part of an analysis of spatial variations in carbon dioxide in L. Janauacá (Amaral et al., 2021) and illustrate the potential influence of lateral exchanges and advection on dissolved gas concentrations. In the embayment, the presence of floating plants fringing open water led to

Table 8

Root-Mean-Square Errors for Calibrated Simulations of Near-Surface and Near-Bottom Dissolved Oxygen Concentrations (mg L^{-1}) at Different Water Levels in Lake Janauacá, Main Lake and Embayment Based on 10-Minute Readings of Moored DO Sensors

Site	Main lake					Embayment				
Year	2015	2015	2015	2016	2016	2015	2015	2015	2016	2016
Month	Mar	Jun	Oct	Jan	Aug	Feb	Jun	Oct	Jan	Aug
Surface DO (mg L^{-1})	1.3	0.9	3.7	1.4	1.4	1.9	1.6	2.2	1.0	4.4
Near-bottom DO (mg L^{-1})	1.0	0.8	4.8	0.6	1.4	1.2	0.1	2.6	0.4	8.6

Note. If lower water column was anoxic, deepest DO sensor was just above oxycline.

differential heating and cooling that resulted in diel changes in the direction and depths of lateral flows. In the open lake, exchange between the littoral and offshore zones occurred at the surface and interior of the lake, and were moderated by wind direction, temperature differences and internal wave motions. A similar approach using methane concentrations in floating plants or flooded forests as transported and dispersed by AEM3D could be done.

4.1.2. Biogeochemical Models of Fluxes and Processes

4.1.2.1. Diffusive Methane Flux

Emission of methane by diffusive flux depends on the concentration gradient near the air-water interface and on the gas transfer velocity that depends on turbulence as a function of heating, cooling and wind speed. The revised version of ALBM uses a formulation of the gas transfer velocity that uses ε, an improvement especially relevant to warm water conditions (MacIntyre et al., 2019, 2021). Previous versions of ALBM used empirically derived relations with wind speed (Riera et al., 1999) or wind speed and thermal conditions in the lake (Heiskanen et al., 2015) derived with data from northern lakes. These formulations do not represent the enhanced turbulence observed under strong near-surface stratification in tropical lakes and other warm waters.

4.1.2.2. Ebullition

The release of methane via bubbles depends on processes in the sediments and overlying water. Given the importance and wide variation in ebullition reported for Amazon floodplain lakes (Barbosa et al., 2021), the mixed success in simulating these fluxes raises concerns regarding the processes modeled or not included. Once methane concentrations in the pore water reaches saturation, bubbles are initiated. Porosity of the sediments, based on a study of two Amazon lakes by Devol et al. (1984), was included. However, release of bubbles may also be influenced by variations in hydrostatic pressure caused by decreases in atmospheric pressure or water level, by bottom-shear owed to currents or waves, or possibly by disturbances from fish or benthic invertebrates (as summarized in Barbosa et al., 2021). These processes are not represented in the current model. Tang et al. (2010) illustrated effects of variations in water level and atmospheric pressure on ebullition in modifications of a process-based wetland model. Barbosa et al. (2021) show an exponentially increasing rate of ebullition as water levels fall at increasing rates with data for Lake Janauacá.

The rising and dissolution of bubbles through the water column are based on equations developed for oceans, as described by Tan et al. (2015). A suite of physical processes including how hydrostatic pressure influences rise rates, bubble expansion and exchange with water in relation to pressure differences and surface tension, could be added, though doing so requires new parameterizations and assumptions. An alternative approach is provided by McGinnis et al. (2006) and Langenegger et al. (2019).

4.1.2.3. Methane Production

Several factors influence the production of methane, including temperature, supply and metabolic availability of organic matter, redox conditions and microbial activity (Bridgham et al., 2013; Grasset et al., 2021; D'Ambrosio & Harrison, 2022). ALBM used temperatures based on measurements and thermal simulations, and Q_{10} for relevant processes were obtained from the literature or calibrated. The type and fraction of sediment utilized for methane production in Amazon lakes is not known and was not differentiated by the model. Furthermore, the nature of microbial communities and their influence on methane production are not known for Amazon lakes.

Using chambers deployed over sediments with water slowly circulating within the chamber, Smith-Morrill (1987) measured methane fluxes from sediments under anoxic water in Lake Calado, an Amazon floodplain lake similar to Lake Janauacá, of ~30–50 mmol CH_4 m^{-2} d^{-1}. This flux is indicative of methanogenesis in the sediments, though not actual rates of methanogenesis. Given the variations of sediments on Amazon floodplains, further studies will likely reveal different methane production rates associated with different sediments (Guyot et al., 2007; Hedges et al., 1986; Martinelli et al., 2003; Moreira-Turcq et al., 2013; Smith et al., 2003). However, as reviewed by D'Ambrosio and Harrison (2022), a wide range of approaches, including sediment incubations, benthic chambers, and models, have been utilized to estimate methane and production and sediment fluxes, all of which have limitations.

4.1.2.4. Methane Oxidation Under oxic Conditions

Simulated rates of methane oxidation varied among seasons and between the main lake and embayment (Table S4 in Supporting Information S1). These results are considerably lower, with a few exceptions, than measurements of methane oxidation in oxic water of the main lake and embayment in Lake Janauacá during rising, high, falling and low water levels reported by Barbosa et al. (2018). In that study, CH_4 oxidation was measured as the CH_4 concentration decline over time following the procedure proposed by Utsumi et al. (1998). Volumetric CH_4 oxidation rates ranged from 0.4 to 11 mmol CH_4 m^{-3} d^{-1}, averaging 2.8 mmol CH_4 m^{-3} d^{-1} in the embayment and from 0.1 to 5 mmol CH_4 m^{-3} d^{-1}, averaging 1.8 mmol CH_4 m^{-3} d^{-1}in the main lake. Rates were higher near the oxycline. Depth-integrated rates averaged 9.1 mmol CH_4 m^{-2} d^{-1} in the embayment and 15.7 mmol CH_4 m^{-2} d^{-1} in the main lake, which often had a deeper oxic zone.

Methane concentrations, dissolved oxygen and temperature are included in the algorithm used for methane oxidation. The range of values used to bound the calibration of O_{max} are from Barbosa et al. (2018), and the calibrated values range over an order of magnitude (Tables 3 and 4). The fixed values of the Michaelis-Menten constants (k_{O_2} and k_{CH_4}) are from Seger's (1998) literature review and a calibrated value derived for a study of boreal lakes (Guo et al., 2020); these may need further modification for the conditions in tropical floodplain lakes. For example, methane oxidation rates decreased by 25%–60% as k_{O_2} varied from 50,000 to 150,000; the fixed value used was 78,000.

Barbosa et al. (2018) found a positive relation between volumetric rates of methane oxidation (Mox, expressed as mg C m^{-3} d^{-1}) and initial dissolved CH_4 concentrations ($[CH_4]$, expressed as μmol L^{-1}). An incorrect equation is shown in Barbosa et al. (2018) for this relation; the correct equation is $\mathrm{Mox} = 65.8\ [CH_4]\ -1.4$. Thottathil et al. (2019) developed a model of the kinetics of CH_4 oxidation based on temperature, CH_4 concentrations and non-linear effect of DO concentrations, expressed by an equation in general and with the fitted parameters specific to a set of northern lakes. The applicability of this relation to other types of lakes has yet to be tested.

Further complexity is indicated by the observations of Morana et al. (2020) that methanotrophy was decreased as sunlight increased in tropical African lakes.

4.1.2.5. Processes Influencing DO Concentrations

Methane production and oxidation are influenced by DO concentrations, which result from processes supplying or consuming DO, including algal photosynthesis, methane oxidation, water-column respiration and SOD plus exchange with the atmosphere. Several modifications were made to the algorithms modeling DO changes in ALBM to suit conditions in tropical floodplain lakes. One difference from previous versions of ALBM is the use of chlorophyll-a concentrations and expressing processes per Chla. Instead of modeling growth and losses of small-sized (e.g., cyanobacteria) and large-sized (e.g., diatoms) phytoplankton, measured Chla concentrations are an input, and chlorophyll-specific rates of photosynthesis and community respiration are incorporated into the model and calibrated with field data. In addition, SOD was added given the warm temperatures, shallow water and organic-rich sediments in tropical floodplain lakes.

Simulated rates of photosynthesis varied among seasons and between the main lake and embayment (Table S5 in Supporting Information S1). These results are generally lower than measurements in Lake Janauacá and in several similar lakes. Amaral et al. (2018) reported rates of planktonic photosynthesis in Lake Janauacá from 67 to 2,950 mmol O_2 m^{-2} d^{-1} spanning the period from September 2015 to May 2016 in the main lake and embayment. Forsberg et al. (2017) reported areal photosynthetic rates of 95 ± 65 (±SD, $n = 90$; range 4.7–361) mmol O_2 $m^{-2}d^{-1}$ for Amazon floodplain lakes influenced by sediment and nutrient-rich rivers.

Simulated rates of photosynthesis are based on simplified equations and parameter values from several sources. Ph_{max} values are within the range reported by Forsberg et al. (2017). The light inhibition and limitation coefficients (K_I and K_2) are based on laboratory incubations at a series of temperatures and light levels of phytoplankton and are unlikely to be appropriate for the phytoplankton in Amazon floodplain lakes.

Simulated rates of planktonic respiration varied among seasons and between the main lake and embayment (Table S6 in Supporting Information S1). Some results are similar and others different from measurements in Lake Janauacá reported by Amaral et al. (2018) and for several similar lakes surveyed by Forsberg et al. (2017). For example, Amaral et al. (2018) reported rates of aerobic plankton respiration in Lake Janauacá of 97 mmol O_2 m^{-3} d^{-1} in the lake and 56 mmol O_2 m^{-3} d^{-1} in the embayment. For Amazon floodplain lakes influenced by sediment and nutrient-rich rivers Forsberg et al. (2017) reported volumetric respiration rates of 48 ± 30 (±SD, $n = 97$; range 7.5–210) mmol O_2 $m^{-3}d^{-1}$ and areal rates of 193 ± 118 (±SD, $n = 95$; range 14–525) mmol O_2 $m^{-2}d^{-1}$. Additional estimates of water-column respiration reported by Vidal et al. (2015) in five

Amazon floodplain lakes ranged from ∼0.5 to 1.5 mmol O_2 m^{-3} h^{-1} during high water and from 0.6 to 4.3 mmol O_2 m^{-3} h^{-1} during low water; as 24-hr totals, these rates are similar to those by Forsberg et al. (2017) and Amaral et al. (2018).

Sediment oxygen demand depends on the nature of the sediments and whether the overlying water is anoxic or oxic. The sediments of Amazon floodplain lakes sequester some organic carbon and release CO_2 and CH_4 to the overlying as a portion of the sedimented carbon is metabolized (Melack & Engle, 2010). As an indication of microbial activity in sediments, a simple model of diagenesis for two small Amazon lakes estimated 6 and 24 mmol m^{-2} d^{-1} of carbon being oxidized (Devol et al., 1984). Using submerged chambers in an Amazon floodplain lake similar to Lake Janauacá, Smith-Morrill (1987) measured dissolved oxygen uptake during periods when the near-bottom waters were aerobic of ∼50 mmol m^{-2} d^{-1}. For comparison, k_s values from Stefan and Fang (1994; Table 2), converted to mmol m^{-2} d^{-1}, are 47 and 310. Simulated SOD values are expressed per m^{-3} as an effect on the overlying water, as noted in the Results.

During all simulated periods daily total DO fluxes were from the atmospheric into the water. As examples for the periods illustrated in Figures 6 and 7, fluxes into the embayment were 53 mmol m^{-2} d^{-1} (Jun 2015) and 160 mmol m^{-2} d^{-1} (Jan 2016), and fluxes into the main lake were 166 mmol m^{-2} d^{-1} (Jun 2015) and 10 mmol m^{-2} d^{-1} (Oct 2015). During low water in October 2015, Chla concentrations were higher (58 μg L^{-1}) than other periods, resulting in elevated photosynthesis during day (Table S5 in Supporting Information S1) with periods of DO fluxes from the lake to the atmosphere, reducing the total daily flux into the lake. DO input from the atmosphere is often higher than photosynthetic DO production and is an important term among the terms influencing DO concentrations.

4.1.2.6. Diel Variations

Diel cycles of stratification and mixing influence the fluxes of methane by changing the vertical distribution of dissolved methane and oxygen and gas exchange across the air-water interface. Diel patterns of stratification and mixing are characteristic of shallow tropical waters, and are conspicuous in Lake Janauacá for temperatures, dissolved oxygen and methane (Figures 6 and 7, Figures S2, S3, S6, S7 in Supporting Information S1). Measurements in Lake Janauacá indicate that near-surface CH_4 concentrations, fluxes and gas exchange velocities were variable over 24-hr periods (Barbosa et al., 2020). Values were higher during the day, but a statistically significant difference between day and night was only found for diffusive fluxes in the embayment. This result is consistent with the day-night differences in wind speed, that were statistically significantly higher during the day. Visual inspection of Figures 4 and 5, Figures S1 and S9 in Supporting Information S1 is suggestive of day-night differences for some periods, and also considerable temporal variability per hour. We did not perform extended simulations to allow a quantitative analysis of day-night proportions.

4.2. Challenges and Limitations of Models

4.2.1. Structural and Numerical Modeling Issues

As noted by Arhonditsis et al. (2008) and others, because ecological processes can be described by a variety of mathematical relations, and given the uncertainty underlying model structures and data, a single set of parameter values, applicable generally, is not a reasonable expectation, that is, the model equifinality. Instead, evaluation of possible inputs, model structures and parameter values on simulated results is necessary (e.g., Tang & Zhuang, 2008). The sensitivity analyses included demonstrate the relative importance of simulated processes. The ranges of values considered for calibration are based on literature values and, in a few cases, results for Amazon floodplains. Moreover, given the large seasonal variations in environmental conditions, calibrations were done for different hydrological periods, instead of assuming constant values. Although our model simulations reproduce well the observations at our study sites, extrapolating the set of parameters obtained to other Amazon lakes and floodplains remains a challenge. A spatially explicit based model parameterization (e.g., Chen & Zhuang, 2012) might be needed given the heterogeneous Amazonia landscapes. Also, because the calibrated parameters are part of functional relations or rates that are derived from fairly complicated biological measurements, to fully account for the effects of the uncertainties of the observational and experimental data, would require incorporation of insufficiently known quantitative and qualitative uncertainties into the Bayesian calibration.

4.2.2. Methane Fluxes and Related Processes

Seasonal diffusive methane fluxes were simulated well in comparison to field measurements, though short-term temporal variability was represented less well. The veracity of simulated ebullition is less clear given the paucity of comparative field data and the episodic nature of ebullition. Simulated methane oxidation rates were often considerably lower than measured rates which suggests revised coefficients or algorithms are needed. Methanogenesis in sediments is a complex process influenced by biological and chemical conditions with few measurements of in situ rates available for comparison. Hence, the simple parameterization used will depend on further studies for improvement. Three-dimensional results from hydrodynamic modeling, such as advective exchanges with fringing habitats and spatial differences in mixed layer depths and turbulence, could enhance the estimates of methane concentrations and fluxes. Further evaluation of the algorithms used in AEM3D to estimate TKE, and the use of TKE in gas exchange and mixing calculations are recommended.

Several biogeochemical aspects of methane production and consumption are not included in the model. The production of CH_4 via the CO_2 reduction pathway or acetoclastic methanogenesis and associated differences in isotopic fractionation, and the composition of microbial communities active in methane processes are not represented. Methane production in oxic waters has been detected (e.g., Grossart et al., 2011), with several mechanisms supporting the process suggested (Bartosiewicz et al., 2022). However, as is evident in the exchange between Günthel et al. (2021) and Peeters and Hofmann (2021), even in well studied lakes, the magnitude of oxic methane production requires further study that combines analyses of physical and biological processes. Although stable isotope tracer experiments in five tropical African lakes indicated an association of oxic CH_4 production and phytoplankton metabolism, CH_4 emissions to the atmosphere were predominantly supported by CH_4 generated in sediments and physically transported to near-surface waters (Morana et al., 2020). Anaerobic oxidation of methane (AOM) can occur in marine and freshwater sediments and depends on availability of terminal electron acceptors such as sulfate, nitrate, iron, manganese and organic acids (Knittel & Boetius, 2009; Reed et al., 2017; Roland et al., 2021). For example, Martinez-Cruz et al. (2018) measured potential rates of AOM based on incubations of sediment slurries spiked with $^{13}CH_4$ from arctic, temperate and tropical lakes. The importance of AOM in lakes and reservoirs is uncertain and depends on several interacting chemical, physical and microbial processes not well constrained with available data. In sediments of Amazon floodplain lakes, concentrations of potential terminal electron acceptors in lake and pore waters are low (Furch, 1997), though AOM could be occurring.

4.2.3. Regionalization in Time and Space

Key challenges to regionalization of methane fluxes in the Amazon basin are the large seasonal variation in inundated areas and habitats, the wide variety of aquatic ecosystems throughout the Amazon basin, and the variability in methane fluxes in time and space (Melack et al., 2022). Models, such as those discussed here, offer one approach to regionalization of methane fluxes. To do so would entail seasonal and annual simulations that require modification of the hydrodynamic and biogeochemical models to run efficiently for longer times and with different inputs than in the versions presented. Downscaled reanalysis meteorological products can be utilized. Remote sensing estimates of inundation at multiple temporal and spatial scales are now available (Fassoni-Andrade et al., 2021; Fleischmann et al., 2021; Parrens et al., 2019). Incorporation of hydrological and hydraulic models of inundation are also essential, and several such models are available and have been applied successfully to the Amazon basin (Ji et al., 2019; Paiva et al., 2013; Rudorff et al., 2014).

Though several wetland models have been applied to Amazon wetlands, these are not well designed for the conditions on floodplains. For example, the Joint UK Land Environment Simulator (JULES) (Clark et al., 2011), the Lund-Potsdam-Jena model (LPJ-WSL; Zhang et al., 2016), LPX-Bern model (Ringeval et al., 2014), and WetCHARTs (Bloom et al., 2017), do not explicitly include methanogenesis, methane oxidation, mixing through the water, ebullition, or air-water exchange. In these models, grid-average methane fluxes are controlled by soil temperature and carbon availability or heterotrophic respiration. Walter and Heimann (2000), TEM-MDM (Zhuang et al., 2004), JPL-WHyMe (Wania et al., 2010) and CLM4Me (Riley et al., 2011) model diffusive emission as molecular diffusion through soil layers.

Optical and trophic conditions vary considerably among Amazon floodplain lakes (Melack et al., 2009, 2021). Hence, simulations of methane fluxes from lakes throughout the region will require modifying parameter values and inputs from those used for Lake Janauacá. In addition to incorporation of data from field studies, remote sensing offers approaches for estimating chlorophyll, suspended sediment and dissolved organic matter concentrations, though the optically complex waters add analytical difficulty and uncertainty (Fassoni-Andrade & Paiva, 2019; Novo et al., 2006; Sayers et al., 2015; Silva et al., 2019).

Another difficulty is the variable mosaic of habitats, including open water, flooded forests, and floating herbaceous plants, as inundation changes through the year (Hess et al., 2015; Melack & Hess, 2010). Floodplain bathymetry is an essential aspect of the occurrence and variations in these habitats, and remote sensing techniques can be used to estimate bathymetry (Fassoni-Andrade et al., 2020). A more complete model needs to incorporate temporal changes in habitat areas and water levels and lateral exchanges between interconnected habitats to calculate methane emissions. Furthermore, environmental conditions and processes influencing methane fluxes differ among open water and inundated vegetated areas as shown by fluxes from water surfaces in floating herbaceous plants and flooded forests measured by Barbosa et al. (2020) and from tree trunks by Pangala et al. (2017) and Gauci et al. (2021). However, modeling plant-mediated transport is premature given the lack of a mechanistic understanding of the processes, large diversity of plants and highly variable fluxes, though clearly needed as relevant information becomes available. Additionally, as water levels fall, large areas shift to unflooded land with extensive areas of woody and herbaceous vegetation and exposed sediments. Models of methane uptake or release by soils and possibly via plants under these conditions could be adapted from terrestrial models such as TEM (Liu et al., 2020; Tang et al., 2010; Zhuang et al., 2013). Therefore, a comprehensive model of methane fluxes associated with Amazon floodplains requires further model developments.

Appendix A: Terms and Names of Modeled and Physical Variables, and Parameters and Coefficients

Terms and names of modeled and physical variables, and parameters and coefficients are listed for fixed values (*) and # calibrated (#) values. Units are shown as usually reported, not at time-step of simulations.

Term Name, units

P	Methanogenesis in sediment, $u$mol m^{-2}s^{-1}
Rc	#Carbon mineralization rate, $u$mol m^{-2}s^{-1}
α_z	#Coefficient of decrease in P with sediment depth, unitless
PQ_{10}	#Q$_{10}$ factor for P, unitless
T_s	Sediment temperature, °C
T_{p0}	*Reference temperature for P, °C
z_s	Depth in sediment, m
C_{CH_4s}	Methane concentration in sediment, μmol L^{-1}
K_{ms}	*Molecular diffusivity in sediment, m^2 s^{-1}
α_{CH_4}	Percentage of methane in bubbles, %
E_s	Ebullition, mmol m^{-2} d^{-1}
α_e	#Saturation level of sediment methane concentration, unitless fraction
C_{CH_4w}	Methane concentration in water column, μmol L^{-1}
t	Time, s
K_z	Eddy diffusivity, m^2 s^{-1}
K_m	*Molecular diffusivity. m^2 s^{-1}
E_{CH_4w}	Gas exchange with bubbles, $u$mol m^{-3} s^{-1}
F_{met}	Diffusive methane flux at water-air interface, μ mol m^{-2} h^{-1}
z	Depth in water, m
ε	Dissipation rate of turbulent kinetic energy, m^2 s^{-3}
N	Brunt-Vaisala frequency, s^{-1}
ρ	Density of water, kg m^{-3}
O	Aerobic methane oxidation, $u$mol m^{-3} s^{-1}
$O_{\max}$	#Methane oxidation potential, μmolm^{-3}s^{-1}
OQ_{10}	*Q_{10} factor for O, unitless
T_w	Water temperature, °C
T_{O0}	*Reference temperature for O, °C
k_{O_2}	*Michaelis-Menten constant for O, $u$mol m^{-3}
k_{CH_4}	*Michaelis-Menten constant for O, $u$mol m^{-3}

C_{O_2}	Concentration of dissolved oxygen in water column, mg L^{-1}
Ph	Oxygen production by photosynthesis, mg L^{-1}
R	Community respiration, mg L^{-1}
SOD	Sediment oxygen demand, mg m^{-2} h^{-1}
F_{oxg}	Oxygen exchange at air-water interface, mg m^{-2} h^{-1}
$Ph_{\max}$	#Chla-specific light-saturation rate of photosynthesis, mg O_2(mg Chla)$^{-1}$$s^{-1}$
θ_p	*Temperature coefficient for photosynthesis, unitless
I	Incident irradiance, μmol photons m^{-2} s^{-1}
C_{Chla}	Chla concentration, mg Chla m^{-3}
K_1	*Light inhibition coefficient, mol m^{-2} s^{-1}
K_2	*Light limitation coefficients, mol m^{-2} s^{-1}
R_r	#Chla-specific respiration rate at 30°C, mg O_2(mg Chla)$^{-1}$$s^{-1}$
θ_r	*Temperature coefficient for respiration, unitless
k_s	#Sediment oxygen demand at 20°C, mg$O_2$$m^{-2}$$s^{-1}$
θ_s	*Temperature coefficient for SOD, unitless
A	Sediment area, m^2
F	Diffusive gas flux at the air-water interface, μmol m^{-2} h^{-1}
k_{600}	Gas transfer velocity normalized to CO_2 at 20°C, cm h^{-1}
C_w	Near-surface gas concentration, μmol L^{-1}
C_{ea}	Near-surface concentration in equilibrium with atmosphere, μmol L^{-1}
υ	Kinematic viscosity, m^2 s^{-1}
Sc	Schmidt number, unitless

Data Availability Statement

Measurements and simulated results presented are available from the KNB data repository operated by NCEAS at https://doi.org/10.5063/F1833QFM (Guo et al., 2023). The revised ALBM code is available from the Purdue Research Repository at https://doi.org/10.4231/4WN4-S032 (Guo & Zhuang, 2023).

Acknowledgments

This study was supported by funding to JMM from NASA grant NNX17AK49G and the US National Science Foundation (NSF DEB Grant 1753856), and funding to QZ by NASA GRANT NNX17AK20G.

References

Amaral, J. H. F., Borges, A. V., Melack, J. M., Sarmento, H., Barbosa, P. M., Kasper, D., et al. (2018). Influence of plankton metabolism and mixing depth on CO_2 dynamics in an Amazon floodplain lake. *Science of the Total Environment*, *630*, 1381–1393. https://doi.org/10.1016/j.scitotenv.2018.02.331

Amaral, J. H. F., Melack, J. M., Barbosa, P. M., Borges, A. V., Kasper, D., Cortés, A. C., et al. (2021). Inundation, hydrodynamics and vegetation influences carbon dioxide concentrations in Amazon floodplain lakes. *Ecosystems*, *25*(4), 911–930. https://doi.org/10.1007/s10021-021-00692-y

Ambrose, R. B. (1988). In *WASP4, a hydrodynamic and water quality model: Model theory, user's manual and programmer's guide* (Vol. 600, pp. 3–39). Environmental Research Laboratory.

Arhonditsis, G. B., Perhar, G., Zhang, W., Massos, E., Shi, M., & Das, A. D. (2008). Addressing equifinality and uncertainty in eutrophication models. *Water Resources Research*, *44*(1), W01420. https://doi.org/10.1029/2007WR005862

Baird, A. J., Beckwith, C. W., Waldron, S., & Waddington, J. M. (2004). Ebullition of methane-containing gas bubbles from near-surface Sphagnum peat. *Geophysical Research Letters*, *31*(21), L21505. https://doi.org/10.1029/2004GL021157

Barbosa, P. M., Farjalla, V. F., Melack, J. M., Amaral, J. H. F., & da Silva, J. S. (2018). High rates of methane oxidation in an Amazon floodplain lake. *Biogeochemistry*, *137*(3), 351–365. https://doi.org/10.1007/s10533-018-0425-2

Barbosa, P. M., Melack, J. M., Amaral, J. H., MacIntyre, S., Kasper, D., Cortés, A., et al. (2020). Dissolved methane concentrations and fluxes to the atmosphere from a tropical floodplain lake. *Biogeochemistry*, *148*(2), 129–151. https://doi.org/10.1007/s10533-020-00650-1

Barbosa, P. M., Melack, J. M., Amaral, J. H. F., Linkhorst, A., & Forsberg, B. R. (2021). Large seasonal and habitat differences in methane ebullition on Amazon floodplains. *Journal of Geophysical Research: Biogeosciences*, *126*(7), e2020JG005911. https://doi.org/10.1029/2020jg005911

Bartosiewicz, M., Venetz, J., Läubli, S., Steiner, O. S., Bouffard, D., Zopfi, J., & Lehmann, M. F. (2023). Detritus-hosted methanogenesis sustains the methane paradox in an alpine lake. *Limnology & Oceanography*, *68*(1), 248–264. https://doi.org/10.1002/lno.12263

Basso, L. S., Marani, L., Gatti, L. V., Miller, J. B., Gloor, M., Melack, J., et al. (2021). Amazon methane budget derived from multi-year airborne observations highlights regional variations in emissions. *Communications Earth & Environment*, *2*(1), 246. https://doi.org/10.1038/s43247-021-00314-4

Beck, V., Chen, H., Gerbig, C., Bergamaschi, P., Bruhwiler, L., Houweling, S., et al. (2012). Methane airborne measurements and comparison to global models during BARCA. *Journal of Geophysical Research*, *117*(D15), D15310. https://doi.org/10.1029/2011JD017345

Bloom, A. A., Bowman, K. W., Lee, M., Turner, A. J., Schroeder, R., Worden, J. R., et al. (2017). A global wetland methane emissions and uncertainty dataset for atmospheric chemical transport models (WetCHARTs version 1.0). *Geoscientific Model Development*, *10*(6), 2141–2156. https://doi.org/10.5194/gmd-10-2141-2017

Bridgham, S. D., Cadillo-Quiroz, H., Keller, J. K., & Zhuang, Q. (2013). Methane emissions from wetlands: Biogeochemical, microbial, and modeling perspectives from local to global scales. *Global Change Biology*, *19*(5), 1325–1346. https://doi.org/10.1111/gcb.12131

Casulli, V., & Cheng, R. T. (1992). Semi-implicit finite difference methods for three-dimensional shallow water flow. *International Journal for Numerical Methods in Fluids*, *15*(6), 629–648. https://doi.org/10.1002/fld.1650150602

Chen, M., & Zhuang, Q. (2012). Spatially explicit parameterization of a terrestrial ecosystem model and its application to the quantification of carbon dynamics of forest ecosystems in the conterminous United States. *Earth Interactions*, *16*(5), 1–22. https://doi.org/10.1175/2012EI400.1

Choubin, B., Zehtabian, G., Azareh, A., Rafiei-Sardooi, E., Sajedi-Hosseini, F., & Kişi, Ö. (2018). Precipitation forecasting using classification and regression trees (CART) model: A comparative study of different approaches. *Environmental Earth Sciences*, *77*(8), 314. https://doi.org/10.1007/s12665-018-7498-z

Clark, D. B., Mercado, L. M., Sitch, S., Jones, C. D., Gedney, N., Best, M. J., et al. (2011). The Joint UK land environment simulator (JULES), model description–Part 2: Carbon fluxes and vegetation dynamics. *Geoscientific Model Development*, *4*(3), 701–722. https://doi.org/10.5194/gmd-4-701-2011

D'Ambrosio, S. L., & Harrison, J. A. (2022). Measuring CH_4 fluxes from lake and reservoir sediments: Methodologies and needs. *Frontiers in Environmental Science*, *10*, 850070. https://doi.org/10.3389/fenvs.2022.850070

DelSontro, T., Beaulieu, J. J., & Downing, J. A. (2016). Greenhouse gas emissions from lakes and impoundments: Upscaling in the face of global change. *Limnology and Oceanography Letters*, *3*, 64–75. https://doi.org/10.1002/lol2.10073

Devol, A. H., Zaret, T. M., & Forsberg, B. R. (1984). Sedimentary organic matter diagenesis and its relation to the carbon budget of tropical Amazon floodplain lakes. *Internationale Vereinigung für theoretische und angewandte Limnologie: Verhandlungen*, *22*(2), 1299–1304. https://doi.org/10.1080/03680770.1983.11897489

Duc, N. T., Crill, P., & Bastviken, D. (2010). Implications of temperature and sediment characteristics on methane formation and oxidation in lake sediments. *Biogeochemistry*, *100*(1–3), 185–196. https://doi.org/10.1007/s10533-010-9415-8

Fassoni-Andrade, A. C., Fleischmann, A. S., Papa, F., Paiva, R. C. D., Wongchuig, S., Melack, J. M., et al. (2021). Amazon hydrology from space: Scientific advances and future challenges. *Reviews of Geophysics*, *59*(4), e2020RG000728. https://doi.org/10.1029/2020RG000728

Fassoni-Andrade, A. C., & Paiva, R. C. D. (2019). Mapping spatial-temporal sediment dynamics of river-floodplains in the Amazon. *Remote Sensing of Environment*, *221*, 94–107. https://doi.org/10.1016/j.rse.2018.10.038

Fassoni-Andrade, A. C., Paiva, R. C. D., Rudorff, C. M., Barbosa, C. C. F., & Novo, E. M. L. M. (2020). High-resolution mapping of floodplain topography from space: A case study in the Amazon. *Remote Sensing of Environment*, *251*, 112065. https://doi.org/10.1016/j.rse.2020.112065

Fleischmann, A. S., Papa, F., Fassoni-Andrade, A., Melack, J. M., Wongchuig, S., Paiva, R. C. D., et al. (2021). How much inundation occurs in the Amazon river basin? *Remote Sensing of Environment*, *278*, 113099. https://doi.org/10.1016/j.rse.2022.113099

Forsberg, B. R., Melack, J. M., Richey, J. E., & Pimentel, T. P. (2017). Regional and seasonal variability in planktonic photosynthesis and planktonic community respiration in Amazon floodplain lakes. *Hydrobiologia*, *800*(1), 187–206. https://doi.org/10.1007/s10750-017-3222-3

Friedman, J. H. (2001). Greedy function approximation: A gradient boosting machine. *Annals of Statistics*, *29*(5), 1189–1232. https://doi.org/10.1214/aos/1013203451

Frieler, K., Lange, S., Piontek, F., Reyer, C. P., Schewe, J., Warszawski, L., et al. (2017). Assessing the impacts of 1.5 C global warming–simulation protocol of the inter-sectoral impact model intercomparison project (ISIMIP2b). *Geoscientific Model Development*, *10*(12), 4321–4345. https://doi.org/10.5194/gmd-10-4321-2017

Furch, K. (1997). Chemistry of várzea and igapó soils and nutrient inventory of their floodplain forests. In W. J. Junk (Ed.), *The central Amazon floodplain* (pp. 47–67). Springer—Verlag.

Gauci, V., Figueiredo, V., Gedney, N., Pangala, S. R., Stauffer, T., Weedon, G. P., & Enrich-Prast, A. (2021). Non-flooded riparian Amazon trees are a regionally significant methane source. *Philosophical Transactions of Royal Society A*, *380*(2215), 20200446. https://doi.org/10.1098/rsta.2020.0446

Grasset, C., Moras, S., Isidorova, A., Couture, R. M., Linkhorst, A., & Sobek, S. (2021). An empirical model to predict methane production in inland water sediment from particular organic matter supply and reactivity. *Limnology & Oceanography*, *66*(10), 3643–3655. https://doi.org/10.1002/lno.11905

Greenwell, B., Boehmke, B., Cunningham, J., Developers, G. B. M., & Greenwell, M. B. (2019). Package 'gbm'. R package version 2.

Grossart, H.-P., Frindte, K., Dziallas, C., Eckert, W., & Tang, K. W. (2011). Microbial methane production in oxygenated water column of an oligotrophic lake. *Proceedings National Academy of Sciences of the United States of America*, *108*(49), 19657–19661. https://doi.org/10.1073/pnas.1110716108

Gudasz, C., Bastviken, D., Steger, K., Premke, K., Sobek, S., & Tranvik, L. J. (2010). Temperature-controlled organic carbon mineralization in lake sediments. *Nature*, *466*(7305), 478–481. https://doi.org/10.1038/nature09186

Günthel, M., Donis, D., Kirillin, G., Ionescu, D., Bizic, M., McGinnis, D. F., et al. (2021). Reply to 'Oxic methanogenesis is only a minor source of lake-wide diffusive CH_4 emissions from lakes. *Nature Communications*, *12*(1), 1205. https://doi.org/10.1038/s41467-021-21216-1

Guo, M., Melack, J., Zhou, W., Barbosa, P., & Amaral, J. (2023). Measured and modeled methane concentration and diffusive methane fluxes at Lake Janauacá (Brazil) between February 2015 and August 2016 [Dataset]. Knowledge Network for Biocomplexity. https://doi.org/10.5063/F1833QFM

Guo, M., & Zhuang, Q. (2023). Linking biogeochemical and hydrodynamic processes to model methane fluxes in shallow, tropical floodplain lakes [Software]. Purdue University Research Repository. https://doi.org/10.4231/4WN4-S032

Guo, M., Zhuang, Q., Tan, Z., Shurpali, N., Juutinen, S., Kortelainen, P., & Martikainen, P. J. (2020). Rising methane emissions from boreal lakes due to increasing ice-free days. *Environmental Research Letters*, *15*(6), 064008. https://doi.org/10.1088/1748-9326/ab8254

Guyot, J. L., Jouanneau, J. M., Soares, L., Boaventura, G. R., Maillet, N., & Lugane, C. (2007). Clay mineral composition of river sediments in the Amazon Basin. *Catena*, *71*(2), 340–356. https://doi.org/10.1016/j.catena.2007.02.002

Harrison, J. A., Prairie, Y. T., Mercier-Blais, S., & Soued, C. (2021). Year-2020 global distribution and pathways of reservoir methane and carbon dioxide emissions according to the greenhouse gas from reservoirs (G-res) model. *Global Biogeochemical Cycles*, *35*(6), e2020GB006888. https://doi.org/10.1029/2020GB006888

Hedges, J. I., Clark, W. A., Quay, P. D., Richey, J. E., Devol, A., & Santos, U. (1986). Composition and fluxes of particulate organic material in the Amazon River. *Limnology & Oceanography*, *31*(4), 717–738. https://doi.org/10.4319/lo.1986.31.4.0717

Heiskanen, J. J., Mammarella, I., Ojala, A., Stepanenko, V., Erkkila, K.-M., Miettinen, H., et al. (2015). Effects of water clarity on lake stratification and lake-atmosphere heat exchange. *Journal of Geophysical Research: Atmospheres*, *120*(15), 7412–7428. https://doi.org/10.1002/2014JD022938

Hess, L. L., Melack, J. M., Affonso, A. G., Barbosa, C., Gastil-Buhl, M., & Novo, E. M. (2015). Wetlands of the lowland Amazon basin: Extent, vegetative cover, and dual-season inundated area as mapped with JERS-1 synthetic aperture radar. *Wetlands*, *35*(4), 745–756. https://doi.org/10.1007/s13157-015-0666-y

Hipsey, M. R., Bruce, L. C., Boon, C., Busch, B., Carey, C. C., Hamilton, D. P., et al. (2019). A general lake model (GLM 3.0) for linking with high-frequency sensor data from the global lake ecological observatory network (GLEON). *Geoscientific Model Development*, *12*(1), 473–523. https://doi.org/10.5194/gmd-12-473-201

Hipsey, M. R., Gal, G., Arhonditsis, G. B., Carey, C. C., Elliott, J. A. M. A., Frassl, M. A., et al. (2020). A system of metrics for the assessment and improvement of aquatic ecosystem models. *Environmental Modelling and Software*, *128*, 104697. https://doi.org/10.1016/j.envsoft.2020.104697

Hodges, B. R. (2000). *Numerical Techniques in CWR-ELCOM (code release v.1)* (p. 37). The University of Western Australia, Center for Water Research.

Hodges, B. R., & Dallimore, C. (2019). *Aquatic ecosystem model: AEM3D, science manual*. Hydronumerics.

Hodges, B. R., Imberger, J., Saggio, A., & Winters, K. B. (2000). Modeling basin-scale internal waves in a stratified lake. *Limnology & Oceanography*, *45*(7), 1603–1620. https://doi.org/10.4319/lo.2000.45.7.1603

Hostetler, S. W., & Bartlein, P. J. (1990). Simulation of lake evaporation with application to modeling lake level variations of Harney-Malheur Lake, Oregon. *Water Resources Research*, *26*(10), 2603–2612. https://doi.org/10.1029/WR026i010p02603

Imberger, J., & Patterson, J. C. (1981). A dynamic reservoir simulation model – DYRESM: 5. In H. B. Fischer (Ed.), *Transport models for inland and coastal waters* (pp. 310–361). Academic Press.

Inglett, K. S., Inglett, P. W., Reddy, K. R., & Osborne, T. Z. (2012). Temperature sensitivity of greenhouse gas production in wetland soils of different vegetation. *Biogeochemistry*, *108*(1–3), 77–90. https://doi.org/10.1007/s10533-011-9573-3

Ji, X., Lesack, L. F. W., Melack, J. M., Wang, S., Riley, W. J., & Shen, C. (2019). Seasonal patterns and controls of hydrological fluxes in an Amazon floodplain lake with a surface-subsurface processes model. *Water Resources Research*, *55*(4), 3056–3075. https://doi.org/10.1029/2018WR023897

Junk, W. J. (1997). *The central Amazon floodplain*. Springer—Verlag. https://doi.org/10.1007/978-3-662-03416-3

Kirschke, S., Bousquet, P., Ciais, P., Saunois, M., Canadell, J. G., Dlugokencky, E. J., et al. (2013). Three decades of global methane sources and sinks. *Nature Geoscience*, *6*(10), 813–823. https://doi.org/10.1038/ngeo1955

Knittel, K., & Boetius, A. (2009). Anaerobic oxidation of methane: Progress with an unknown process. *Annual Review of Microbiology*, *63*(1), 311–334. https://doi.org/10.1146/annurev.micro.61.080706.093130

Knox, S. H., Bansal, S., McNicol, G., Schafer, K., Sturtevant, C., Ueyama, M., et al. (2021). Identifying dominant environmental predictors of freshwater wetland methane fluxes across diurnal to seasonal time scales. *Global Change Biology*, *7*(15), 3582–3604. https://doi.org/10.1111/gcb.15661

Krzywinski, M., & Altman, N. (2017). Classification and regression trees. *Nature Methods*, *14*(8), 757–758. https://doi.org/10.1038/nmeth.4370

Langenegger, T., Vachon, D., Donis, D., & McGinnis, D. F. (2019). What the bubble knows: Lake methane dynamics revealed by sediment gas bubble composition. *Limnology & Oceanography*, *64*(4), 1526–1544. https://doi.org/10.1002/lno.11133

Leonard, B. P. (1991). The ultimate conservative difference scheme applied to unsteady one-dimensional advection. *Computer Methods in Applied Mechanics and Engineering*, *88*(1), 17–74. https://doi.org/10.1016/0045-7825(91)90232-u

Liang, J. H., McWilliams, J. C., Sullivan, P. P., & Baschek, B. (2011). Modeling bubbles and dissolved gases in the ocean. *Journal of Geophysical Research*, *116*(C3), C03015. https://doi.org/10.1029/2010JC006579

Liu, L., Zhuang, Q., Oh, Y., Shurpali, N. J., Kim, S., & Poulter, B. (2020). Uncertainty quantification of global net methane emissions from terrestrial ecosystems using a mechanistically based biogeochemistry model. *Journal of Geophysical Research: Biogeoscience*, *125*(6), e2019JG005428. https://doi.org/10.1029/2019JG005428

MacIntyre, S., Amaral, J. H., Barbosa, P. M., Cortés, A., Forsberg, B. R., & Melack, J. M. (2019). Turbulence and gas transfer velocities in sheltered flooded forests of the Amazon Basin. *Geophysical Research Letters*, *46*(16), 9628–9636. https://doi.org/10.1029/2019gl083948

MacIntyre, S., Amaral, J. H., & Melack, J. M. (2021). Turbulence in the upper mixed layer under light winds: Implications for fluxes of climate-warming trace gases. *Journal of Geophysical Research: Oceans*, *126*(12), e2020JC017026. https://doi.org/10.1029/2020JC017026

MacIntyre, S., & Melack, J. M. (2009). Mixing dynamics in lakes across climatic zones. *Encyclopedia of Inland Waters*, *2*, 603–612. https://doi.org/10.1016/b978-012370626-3.00040-5

Marotta, H., Pinho, L., Gudasz, C., Bastviken, D., Tranvik, L. J., & Enrich-Prast, A. (2014). Greenhouse gas production in low-latitude lake sediments responds strongly to warming. *Nature Climate Change*, *4*(6), 467–470. https://doi.org/10.1038/nclimate2222

Martinelli, L. A., Victoria, R. L., de Camargo, P. B., Piccolo, M. C., Mertes, L., Richey, J. E., et al. (2003). Inland variability of carbon–nitrogen concentrations and δ13C in Amazon floodplain (várzea) vegetation and sediment. *Hydrological Processes*, *17*(7), 1419–1430. https://doi.org/10.1002/hyp.1293

Martinez-Cruz, K., Sepulveda-Jauregui, A., Casper, P., Walter Anthony, K., Smemo, K. A., & Thalasso, F. (2018). Ubiquitous and significant anaerobic oxidation of methane in freshwater lake sediments. *Water Research*, *144*, 332–340. https://doi.org/10.1016/j.watres.2018.07.053

McGinnis, D. F., Greinert, J., Artemov, Y., Beaubien, S. E., & Wüest, J. (2006). Fate of rising methane bubbles in stratified waters: How much methane reaches the atmosphere? *Journal of Geophysical Research*, *111*(C9), 1–15. https://doi.org/10.1029/2005JC003183

Megard, R. O., Tonkyn, D. W., & Senft, W. H. (1984). Kinetics of oxygenic photosynthesis in planktonic algae. *Journal of Plankton Research*, *6*(2), 325–337. https://doi.org/10.1093/plankt/6.2.325

Melack, J. M. (2016). Aquatic ecosystems. In L. Nagy, B. R. Forsberg, & P. Artaxo (Eds.), *Interactions between biosphere, atmosphere and human land use in the Amazon basin, ecological studies* (Vol. 227, pp. 117–145). Springer.

Melack, J. M., Amaral, J. H. F., Kasper, D., Barbosa, P. M., & Forsberg, B. R. (2021). Limnological perspectives on conservation of aquatic ecosystems in the Amazon basin. *Aquatic Conservation: Marine and Freshwater Ecosystems*, *31*(5), 1041–1055. https://doi.org/10.1002/aqc.3556

Melack, J. M., Basso, L. S., Fleischmann, A. S., Botía, S., Guo, M., Zhou, W., et al. (2022). Challenges regionalizing methane emissions using aquatic environments in the Amazon basin as examples. *Frontiers in Environmental Science*, *10*, 866082. https://doi.org/10.3389/fenvs.2022.866082

Melack, J. M., & Engle, D. L. (2010). An organic carbon budget for an Amazon floodplain lake. *Internationale Vereinigung für theoretische und angewandte Limnologie: Verhandlungen*, *30*(8), 1179–1182. https://doi.org/10.1080/03680770.2009.11923906

Melack, J. M., & Hess, L. L. (2010). Remote sensing of the distribution and extent of wetlands in the Amazon basin. In W. J. Junk, M. Piedade, F. Wittmann, J. Schöngart, & P. Parolin (Eds.), *Amazonian floodplain forests: Ecophysiology, ecology, biodiversity and sustainable management, ecological studies* (Vol. 210, pp. 43–59). Springer.

Melack, J. M., Hess, L. L., Gastil, M., Forsberg, B. R., Hamilton, S. K., Lima, I. B., & Novo, E. M. (2004). Regionalization of methane emissions in the Amazon Basin with microwave remote sensing. *Global Change Biology*, *10*(5), 530–544. https://doi.org/10.1111/j.1365-2486.2004.00763.x

Melack, J. M., Novo, E. M. L. M., Forsberg, B. R., Piedade, M. T. F., & Maurice, L. (2009). Floodplain ecosystem processes. In J. Gash, M. Keller, & P. Silva-Dias (Eds.), *Amazonia and global change. Geophysical Monograph Series* (Vol. 186, pp. 525–541). American Geophysical Union.

Melton, J. R., Wania, R., Hodson, E. L., Poulter, B., Ringeval, B., Spahni, R., et al. (2013). Present state of global wetland extent and wetland methane modelling: Conclusions from a model inter-comparison project (WETCHIMP). *Biogeosciences*, *10*(2), 753–788. https://doi.org/10.5194/bg-10-753-2013

Messager, M. L., Lehner, B., Grill, G., Nedeva, I., & Schmitt, O. (2016). Estimating the volume and age of water stored in global lakes using a geo-statistical approach. *Nature Communications*, *7*(1), 13603. https://doi.org/10.1038/ncomms13603

Morana, C., Bouillon, S., Nolla-Ardèvol, V., Roland, F. A. E., Okello, W., Descy, J.-P., et al. (2020). Methane paradox in tropical lakes? Sedimentary fluxes rather than pelagic production in oxic conditions sustain methanotrophy and emissions to the atmosphere. *Biogeosciences*, *17*(20), 5209–5221. https://doi.org/10.5194/bg-17-5209-2020

Moreira-Turcq, P., Bonnet, M. P., Amorim, M., Bernardes, M., Lagane, C., Maurice, L., et al. (2013). Seasonal variability in concentration, composition, age, and fluxes of particulate organic carbon exchanged between the floodplain and Amazon River. *Global Biogeochemical Cycles*, *27*(1), 119–130. https://doi.org/10.1002/gbc.20022

Novo, E. M. L. M., Barbosa, C. C., Freitas, R. M., Shimabukuro, Y. E., Melack, J. M., & Pereira Filho, W. (2006). Seasonal changes in chlorophyll-a distributions in Amazon floodplain lakes derived from MODIS images. *Limnology*, *7*(3), 153–161. https://doi.org/10.1007/s10201-006-017-8

Nzotungicimpaye, C.-M., Zickfeld, K., MacDougall, A. H., Melton, J. R., Treat, C. C., Eby, M., & Lesack, L. F. W. (2021). WETMETH 1.0: A new wetland methane model for implementation in Earth system models. *Geoscientific Model Development*, *14*(10), 6215–6240. https://doi.org/10.5194/gmd-14-6215-2021

Paiva, R. C. D., Buarque, D. C., Collischonn, W., Bonnet, M. P., Frappart, F., Calmant, S., & Mendes, C. A. B. (2013). Large-scale hydrologic and hydrodynamic modeling of the Amazon River basin. *Water Resources Research*, *49*(3), 1226–1243. https://doi.org/10.1002/wrcr.20067

Pangala, S. R., Enrich-Prast, A., Basso, L. S., Peixoto, R. B., Bastviken, D., Hornibrook, E. R., et al. (2017). Large emissions from floodplain trees close the Amazon methane budget. *Nature*, *552*(7684), 230–234. https://doi.org/10.1038/nature24639

Parrens, M., Bitar, A. A., Frappart, F., Paiva, R., Wongchuig, S., Papa, F., et al. (2019). High resolution mapping of inundation area in the Amazon basin from a combination of L-band passive microwave, optical and radar datasets. *International Journal of Applied Earth Observation and Geoinformation*, *81*, 58–71. https://doi.org/10.1016/j.jag.2019.04.011

Peeters, F., & Hofmann, H. (2021). Oxic methanogenesis is only a minor source of lake-wide diffusive CH_4 emissions from lakes. *Nature Communications*, *12*(1), 1206. https://doi.org/10.1038/s41467-021-21215-2

Pekel, J. F., Cottam, A., Gorelick, N., & Belward, A. S. (2016). High-resolution mapping of global surface water and its long-term changes. *Nature*, *540*(7633), 418–422. https://doi.org/10.1038/nature20584

Peng, S., Lin, X., Thompson, R. L., Xi, Y., Liu, G., Hauglustaine, D., et al. (2022). Wetland emission and atmospheric sink changes explain methane growth in 2020. *Nature*, *612*(7940), 477–482. https://doi.org/10.1038/s41586-022-05447-w

Pinel, S., Bonnet, M. P., Santos Da Silva, J., Moreira, D., Calmant, S., Satgé, F., & Seyler, F. (2015). Correction of interferometric and vegetation biases in the SRTMGL1 spaceborne DEM with hydrological conditioning towards improved hydrodynamics modeling in the Amazon Basin. *Remote Sensing*, *7*(12), 16108–16130. https://doi.org/10.3390/rs71215822

Potter, C., Melack, J. M., & Engle, D. (2014). Modeling methane emissions from Amazon floodplain ecosystems. *Wetlands*, *34*(3), 501–511. https://doi.org/10.1007/s13157-014-0516-3

Reed, D. C., Deemer, B. R., van Grinsven, S., & Harrison, J. A. (2017). Are elusive anaerobic pathways key methane sinks in eutrophic lakes and reservoirs? *Biogeochemistry*, *134*(1–2), 29–39. https://doi.org/10.1007/s10533-017-0356-3

Riera, J. L., Schindler, J. E., & Kratz, T. K. (1999). Seasonal dynamics of carbon dioxide and methane in two clear-water lakes and two bog lakes in northern Wisconsin, U.S.A. *Canadian Journal of Fisheries and Aquatic Sciences*, *56*(2), 265–274. https://doi.org/10.1139/f98-182

Riley, W. J., Subin, Z. M., Lawrence, D. M., Swenson, S. C., Torn, M. S., Meng, L., et al. (2011). Barriers to predicting changes in global terrestrial methane fluxes: Analyses using CLM4Me, a methane biogeochemistry model integrated in CESM. *Biogeosciences*, *8*(7), 1925–1953. https://doi.org/10.5194/bg-8-1925-2011

Ringeval, B., Houweling, S., Van Bodegom, P. M., Spahni, R., Van Beek, R., Joos, F., & Röckmann, T. (2014). Methane emissions from floodplains in the Amazon Basin: Challenges in developing a process-based model for global applications. *Biogeosciences*, *11*(6), 1519–1558. https://doi.org/10.5194/bg-11-1519-2014

Rodrigues, M., & de la Riva, J. (2014). An insight into machine-learning algorithms to model human-caused wildfire occurrence. *Environmental Modelling & Software*, *57*, 192–201. https://doi.org/10.1016/j.envsoft.2014.03.003

Roland, F. A. E., Borges, A. V., Steven Bouillon, S., & Morana, C. (2021). Nitrate-dependent anaerobic methane oxidation and chemolithotrophic denitrification in a temperate eutrophic lake. *FEMS Microbiology Ecology*, *97*(10). https://doi.org/10.1093/femsec/fiab124

Rosentreter, J. A., Borges, A. V., Deemer, B. R., Holgerson, M. A., Liu, S., Song, C., et al. (2021). Half of global methane emissions come from highly variable aquatic ecosystem sources. *Nature Geoscience*, *14*(4), 225–230. https://doi.org/10.1038/S41561-021-00715-2

Rudorff, C. M., Melack, J. M., & Bates, P. M. (2014). Flooding dynamics on the lower Amazon floodplain: 1. Hydraulic controls on water elevation, inundation extent and river-floodplain discharge. *Water Resources Research*, *50*, 619–634. https://doi.org/10.1002/2013wr014091

Saunois, M., Stavert, A. R., Poulter, B., Bousquet, P., Canadell, J. G., Jackson, R. B., et al. (2020). The global methane budget: 2000-2017. *Earth System Science Data*, *12*(3), 1561–1623. https://doi.org/10.5194/essd-12-1561-2020

Sayers, M. J., Grimm, A. G., Shuchman, R. A., Deines, A. M., Bunnell, D. B., Raymer, Z. B., et al. (2015). A new method to generate a high-resolution global distribution map of lake chlorophyll. *International Journal of Remote Sensing*, *36*(7), 1942–1964. https://doi.org/10.1080/01431161.2015.1029099

Segers, R. (1998). Methane production and methane consumption: A review of processes underlying wetland methane fluxes. *Biogeochemistry*, *41*(1), 23–51. https://doi.org/10.1023/a:1005929032764

Silva, M. P., Sander de Carvalho, L., Novo, E., Jorge, D., & Barbosa, C. (2019). Use of absorption optical indices to assess seasonal variability of dissolved organic matter in Amazon floodplain lakes. *Biogeosciences Discussions*, 1–20. https://doi.org/10.5194/bg-2019-324

Sippel, S. J., Hamilton, S., & Melack, J. M. (1991). Inundation area and morphometry of lakes on the Amazon River floodplain, Brazil. *Archiv für Hydrobiologie*, *123*(4), 385–400. https://doi.org/10.1127/archiv-hydrobiol/123/1992/385

Smith, L. K., Melack, J. M., & Hammond, D. E. (2003). Carbon, nitrogen and phosphorus content and ^{210}Pb-derived burial rates in sediments of an Amazon floodplain lake. *Amazoniana*, *17*, 413–436.

Smith-Morrill, L. (1987). The exchange of carbon, nitrogen, and phosphorus between the sediments and water-column of an Amazon floodplain lake. Ph.D. Thesis (p. 209). University of Maryland.

Sobrinho, R. L., Bernardes, M. C., Abril, G., Kim, J.-H., Zell, C. I., Mortillaro, J.-M., et al. (2016). Spatial and seasonal contrasts of sedimentary organic matter in floodplain lakes of the central Amazon basin. *Biogeosciences*, *13*(2), 467–482. https://doi.org/10.5194/bg-13-467-2016

Spigel, R. H., Imberger, J., & Rayner, K. N. (1986). Modeling the diurnal mixed layer. *Limnology & Oceanography*, *31*(3), 533–556. https://doi.org/10.4319/lo.1986.31.3.0533

Stefan, H. G., & Fang, X. (1994). Dissolved oxygen model for regional lake analysis. *Ecological Modelling*, *71*(1–3), 37–68. https://doi.org/10.1016/0304-3800(94)90075-2

Stepanenko, V., Mammarella, I., Ojala, A., Miettinen, H., Lykosov, V., & Vesala, T. (2016). LAKE 2.0: A model for temperature, methane, carbon dioxide and oxygen dynamics in lakes. *Geoscientific Model Development*, *9*(5), 1977–2006. https://doi.org/10.5194/gmd-9-1977-2016

Subin, Z. M., Riley, W. J., & Mironov, D. (2012). An improved lake model for climate simulations: Model structure, evaluation, and sensitivity analyses in CESM1. *Journal of Advances in Modeling Earth Systems*, *4*(1), M02001. https://doi.org/10.1029/2011MS000072

Talling, J. F., & Lemoalle, J. (1998). *Ecological dynamics of tropical inland waters* (p. 441). Cambridge University Press.

Tan, Z., Zhuang, Q., Shurpali, N. J., Marushchak, M. E., Biasi, C., Eugster, W., & Anthony, K. W. (2017). Modeling CO_2 emissions from Arctic lakes: Model development and site-level study. *Journal of Advances in Modeling Earth Systems*, *9*(5), 2190–2213. https://doi.org/10.1002/2017MS001028

Tan, Z., Zhuang, Q., & Walter Anthony, K. (2015). Modeling methane emissions from arctic lakes: Model development and site-level study. *Journal of Advances in Modeling Earth Systems*, *7*(2), 459–483. https://doi.org/10.1002/2014MS000344

Tang, J., & Zhuang, Q. (2008). Equifinality in parameterization of process-based biogeochemistry models: A significant uncertainty source to the estimation of regional carbon dynamics. *Journal of Geophysical Research*, *113*(G4), G04010. https://doi.org/10.1029/2008JG000757

Tang, J., Zhuang, Q., Shannon, R. D., & White, J. R. (2010). Quantifying wetland methane emissions with process-based models of different complexities. *Biogeosciences*, *7*(11), 3817–3837. https://doi.org/10.5194/bg-7-387-2010

Thottathil, S. D., Reis, P. C. J., & Prairie, Y. T. (2019). Methane oxidation kinetics in northern freshwater lakes. *Biogeochemistry*, *143*(1), 105–116. https://doi.org/10.1007/s10533-019-00552-x

Utsumi, M., Nojiri, Y., Nakamura, T., Nozawa, T., Otsuki, A., Takamura, N., et al. (1998). Dynamics of dissolved methane and methane oxidation in dimictic Lake Nojiri during winter. *Limnology & Oceanography*, *43*(1), 10–17. https://doi.org/10.4319/lo.1998.43.1.0010

Vidal, L. O., Abril, G., Artigas, L. F., Melo, M. L., Bernardes, M. C., Lobão, L. M., et al. (2015). Hydrological pulse regulating the bacterial heterotrophic metabolism between Amazonian mainstems and floodplain lakes. *Frontiers in Microbiology*, *6*, 1054. https://doi.org/10.3389/fmicb.2015.01054

Walter, B. P., & Heimann, M. (2000). A process-based, climate-sensitive model to derive methane emissions from natural wetlands: Application to five wetland sites, sensitivity to model parameters, and climate. *Global Biogeochemical Cycles*, *14*(3), 745–765. https://doi.org/10.1029/1999gb001204

Wania, R., Ross, I., & Prentice, I. C. (2010). Implementation and evaluation of a new methane model within a dynamic global vegetation model: LPJ-WHyMe v1. 3.1. *Geoscientific Model Development*, *3*(2), 565–584. https://doi.org/10.5194/gmd-3-565-2010

Woolf, D. K., & Thorpe, S. A. (1991). Bubbles and the air-sea exchange of gases in near-saturation conditions. *Journal of Marine Research*, *49*(3), 435–466. https://doi.org/10.1357/002224091784995765

Yang, Z., & Dominguez, F. (2019). Investigating land surface effects on the moisture transport over South America with a moisture tagging model. *Journal of Climate*, *52*(19), 6627–6644. https://doi.org/10.1175/JCLI-D-18-0700.1

Yeates, P. S., & Imberger, J. (2003). Pseudo two-dimensional simulations of internal and boundary fluxes in stratified lakes and reservoirs. *International Journal of River Basin Management*, *1*(4), 1–23. https://doi.org/10.1080/15715124.2003.9635214

Zhang, Z., Zimmermann, N. E., Kaplan, J. O., & Poulter, B. (2016). Modeling spatiotemporal dynamics of global wetlands: Comprehensive evaluation of a new sub-grid TOPMODEL parameterization and uncertainties. *Biogeosciences*, *13*(5), 1387–1408. https://doi.org/10.5194/bg-13-1387

Zhou, W., Imberger, J., & Marti, C. L. (2021). A new pseudo three-dimensional hydrodynamic model with Lagrangian vertical mixing and Eulerian horizontal mass exchange. *Environmental Modelling & Software*, *143*, 105099. https://doi.org/10.1016/j.envsoft.2021.105099

Zhuang, Q., Chen, M., Xu, K., Tang, J., Saikawa, E., Lu, Y., et al. (2013). Response of global soil consumption of atmospheric methane to changes in atmospheric climate and nitrogen deposition. *Global Biogeochemical Cycles*, *27*(3), 650–663. https://doi.org/10.1002/gbc.20057

Zhuang, Q., Melillo, J. M., Kicklighter, D. W., Prinn, R. G., McGuire, A. D., Steudler, P. A., et al. (2004). Methane fluxes between terrestrial ecosystems and the atmosphere at northern high latitudes during the past century: A retrospective analysis with a process-based biogeochemistry model. *Global Biogeochemical Cycles*, *18*(3), GB3010. https://doi.org/10.1029/2004GB002239